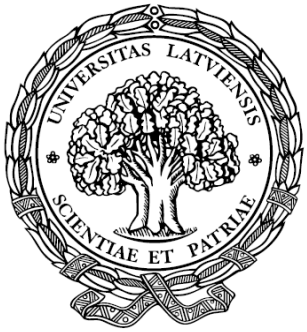

UNIVERSITY OF LATVIA

FACULTY OF PHYSICS AND MATHEMATICS

Andrejs Jarmola

Tunable laser spectroscopy and electric field effects in alkali vapour

Doctoral Thesis

SUMMARY

Riga, 2007

The dissertation work was carried out at the Faculty of Physics and Mathematics of the University of Latvia in the time period from 2001 to 2006.

Type of Work: Collection of scientific articles

Scientific Advisor: *Dr. habil. phys.* RUVINS FERBERS, Professor, University of Latvia

Dissertation Reviewers:

1. IVARS LĀCIS, *Dr. habil. phys.,* Professor, University of Latvia
Name, surname; academic degree; academic position; scientific institution

2. CHRISTINA ANDREEVA, *Dr. phys.*, Researcher, Institute of Electronics, Bulgarian Academy of Sciences

3. EDMUNDS TAMANIS, *Dr. phys.*, Assoc. Professor, Daugavpils University

The dissertation defense will take place in the open session of the Physics and Astronomy Dissertation Commission of the University of Latvia to be held on December 10, 2007, at 16:30 in Room 233 of the Faculty of Physics and Mathematics at Zeļļu Street 8.

The dissertation and its summary are available at the University of Latvia Library (Kalpaka Blvd. 4) and at the Latvian Academic Library (Rūpniecības Street 10).

LU Physics and Astronomy Dissertation Commission chairperson:

Prof. R. Ferbers

Abstract

This thesis is devoted to studies of coherent effects in highly excited levels of Cs atoms in the presence of an external electric field, as well as to investigations of the strongly mixed singlet-triplet $A^1\Sigma^+ - b^3\Pi$ complex of tha NaRb molecule. The experiments were performed in alkali metal vapours by detecting the fluorescence exited by tunable diode and dye lasers

Electric field induced level-crossing signals of m_F magnetic sublevels of the hyperfine F levels have been observed for the first time in atoms in two-step laser excitation, namely for the nD$_{3/2}$ and nD$_{5/2}$ states of Cs with n = 7, 9, and 10. New values of the tensor polarizabilities α_2 and the hyperfine structure constants A for nD Cs states are determined by means of measured level-crossing signals.

Alignment to orientation conversion induced by an external electric field has been observed for the first time in atoms, namely for the 7D$_{3/2}$ and 9D$_{3/2}$ states of Cs. The study of alignment to orientation conversion in atoms is of great interest, since this phenomenon can represent a potential background for electron electric dipole moment searches in atomic or molecular systems.

The possibility of using cesium vapour as a tracer gas to optically image electric field distributions has been demonstrated. The presented technique takes advantage of the fact that the laser induced fluorescence intensity of the nD states of Cs depends on the external electric field strength

The intensity distribution in the NaRb $A^1\Sigma^+ \sim b^3\Pi \rightarrow X\ ^1\Sigma^+$ fluorescence series induced by diode laser excitation from the ground state has been measured and directly applied to restore the adiabatic potential energy curve for the A-state of the fully-mixed $A^1\Sigma^+ \sim b^3\Pi$ complex.

Contents

1. Introduction

The present **Thesis** describes applications of tunable lasers to the study of highly excited levels in atoms in the presence of an external electric field, as well as to the observation of laser induced fluorescence intensity distribution from selectively excited rovibronic levels of mixed singlet-triplet complex of alkali diatomic molecules.

Generally, the work presented in this Thesis can be divided into four parts, (a) study of level-crossing signals in an external electric field at two-step laser excitation in Cs atoms, (b) observation of an electric-field-induced alignment to orientation conversion in Cs atoms, (c) introduction of the method of optical imaging of an external electric field distribution in Cs vapour, and (d) spectroscopy of the NaRb molecule using diode laser radiation.

The perturbation of atomic energy levels by a static external electric or magnetic field is an important tool in atomic spectroscopy. In particular, the influence of these fields leads to the splitting of the magnetic sublevels m_F of hyperfine levels F and causes the sublevels to cross. The technique that uses this level splitting results to determine of atomic properties is called ***level-crossing spectroscopy***. This technique was used in atomic physics even before the invention of lasers [2, 3]. These investigations were, however, restricted to atomic resonance transitions that could be excited with intense hollow-cathode or microwave atomic-resonance lamps. The introduction of tunable lasers drastically increased the number of application of level-crossing spectroscopy to the investigation of highly excited states of atoms, reached in many cases by applying two-step excitation [4-6], in the presence of external magnetic field.

Level-crossing spectroscopy in an external electric field has not been exploited as extensively as in an external magnetic field for the study of atomic structures because of the fact that a homogenous electric field is harder to produce and measure than a magnetic field that causes a comparable magnetic sublevel splitting. A small number of publications exist [7-9] on pure electric field level-crossing studies in atoms at one step. However, the extant literature contains no experimental studies of purely electric field level crossings of magnetic sublevels m_F of hyperfine structure levels F at two-step, or any multi-step, laser excitation.

The study of *electric field induced symmetry breaking of angular momentum distribution* in atoms is of great interest, since such symmetry breaking can represent a potential background for *electron electric dipole moment* (EDM) searches in atomic or molecular systems [10,11]. The most sensitive upper limit to date on the electron EDM has been achieved by searching for a small precession around an external electric field of the

angular momentum distribution of an ensemble of atoms [12]. Various sophisticated experimental techniques prevent angular momentum precession caused by mechanisms other than an EDM from contaminating the signal. One such phenomenon, known as ***alignment to orientation conversion*** (AOC), is known to deform the atomic and molecular angular momentum distributions under the influence of electric and magnetic fields or collisions.

From symmetry considerations, it follows that excitation by linearly polarized light is capable of creating *alignment* of the angular momentum of atoms and is not capable of producing *orientation* of the angular momentum [13]. Nevertheless, these strict symmetry rules can be broken in the presence of external perturbations, such as anisotropic collisions or magnetic and electric fields. The breaking of the reflection symmetry of an initially aligned population of atoms by converting the alignment into transverse orientation (AOC) has been a subject of theoretical and experimental investigation since the 1960s, beginning with the work of [14–17]. The very first theoretical works suggested that AOC may be induced in atoms by a magnetic field gradient [14] or by anisotropic collisions [15, 16]. Later, it was shown theoretically [18-21] that AOC can be induced by a purely electric field without the need for magnetic fields or collisions whenever the initial alignment is not exactly perpendicular or parallel to the external electric field. However, no experimental studies of AOC in atoms in a purely electric field have been reported.

The dependence of the laser induced fluorescence intensity on an external electric field in highly excited states of atoms can be exploited to ***optical image an external electric field distribution***. The first use of Stark spectroscopy to image the spatial dependence of an electric field was carried out by Nakajima *et al* [22]. In 1989 Yang *et al* [23] demonstrated that the Stark effect could be used to achieve precise measurements of electric field strength.

Despite the large number of applications for which a spatial map of electric field strength might be useful, practical applications of the Stark effect to probe electric field distributions have been limited to fields in hostile environments such as plasmas, ovens at high temperatures, and rf discharges. One of the recently suggested successful schemes for electric field measurement [24] takes advantage of the laser induced fluorescence polarization dependence on the electric field of the $B^1\Pi \rightarrow X^1\Sigma$ transition in the NaRb molecule.

In this Thesis the possibility of using cesium vapour to optically image of electric field distributions has been studied. The use of atomic cesium vapour offers the following advantages: low working temperatures, the possibility to implement the method using only diode lasers, ease of separating atomic fluorescence from scattered light using simple optical

filters. The technique could lead to many practical applications, including the testing of digital integrated circuits.

In recent years there has been a growing interest in the formation of ultracold (with translation temperature less than 1 mK) polar molecules. The main motivation is the possibility of controlling and manipulating them with external electric fields. Heteronuclear alkali-metal diatomic molecules are good candidates since they have large permanent electric dipole moments. Also, the formation of ultracold molecules is of particular interest for such fields as: observation of Bose-Einstein condensation, testing of fundamental theories, such as the search for an electric dipole moment of the electron [25, 26]; quantum computation using aligned molecular dipoles as qubits [27].

Recently, the successful production of ultracold NaLi [28], KRb [29-31], NaCs [32], NaRb [33-35], and RbCs [36] heteronuclear dimers was reported. The first promising results for the formation of ultracold heteronuclear diatomic molecules refer mostly to translationally cold ones, which are in highly excited rovibronic levels. Further progress in converting ultracold heteronuclear alkali-metal diatomic molecules to their ground state $v'' = 0$, $J'' = 0$ level could be expected by exploiting stimulated Raman transitions via intermediate levels that belongs to the strongly mixed singlet-triplet $A^1\Sigma^+ - b^3\Pi$ complex as proposed by Stwalley [37]. Therefore, data from the strongly mixed $A^1\Sigma^+ - b^3\Pi$ complex are essential for planning such types of experiments.

The relative intensity distribution of the laser induced fluorescence $A\text{-}b \rightarrow X$ progressions is much less influenced by the strong spin–orbit interaction than by the corresponding term values of the fully coupled $A^1\Sigma^+ - b^3\Pi$ complex. Therefore, the observation of the relative intensity distribution from the strongly mixed $A^1\Sigma^+ - b^3\Pi$ complex to the ground $X^1\Sigma^+$ state may supply a unique clue for performing a partial deperturbation analysis of the strongly mixed states by providing unambiguous vibrational numbering as well as the adiabatic potential energy curve that can be used as the first approximation for further non-adiabatic treatment.

Research objects

The main research objects of the present Thesis are the **Cs** atom and the **NaRb** molecule.

The **Cs** atom is a challenging test object for frontier research, which includes parity non-conservation, laser cooling and BEC, searches for a permanent electric dipole moment of the electron and testing of Zeeman coherence manifestation. The use of atomic Cs offers the advantages: that, already at room temperature, the concentration of cesium atoms is enough to produce a strong LIF signal, therefore highly excited states could be populated be using conventional diode and dye lasers at low working temperatures

The **NaRb** molecule is a prospective candidate for the formation of ultracold heteronuclear diatomic molecules.

Goals

The main goals of the present research are:

1. To study the (nD) states of Cs by observing the pure electric-field-induced level-crossing resonances of m_F Zeeman sublevels of hyperfine F levels while applying two-step laser excitation in order to determine the tensor polarizabilities and the hyperfine structure constants for these states.
2. To observe the alignment to orientation conversion in (nD) states of Cs atoms in the presence of an external dc electric field and without the influence of magnetic fields and atomic collisions.
3. To study the possibility of using the laser induced fluorescence dependence on electric field to map electric field distributions with optical methods.
4. To study the fully-mixed $A^1\Sigma^+$ - $b^3\Pi$ complex of NaRb molecules, applying diode laser excitation and analyzing the relative intensity distribution of the laser induced fluorescence.

Publications

The main results of the Thesis are presented in the following scientific papers:

[dis1] **A. Jarmola**, M. Tamanis, R. Ferber, E.A. Pazyuk, A.V. Stolyarov, *LIF intensity distribution as a deperturbation tool: application to the fully-mixed $A^1S+ - b^3P$ complex of NaRb*, Journal of Quantitative Spectroscopy & Radiative Transfer 95, 165–174 (2005).

[dis2] M. Auzinsh, K. Blushs, R. Ferber, F. Gahbauer, **A. Jarmola**, M. Tamanis, *Electric field induced hyperfine level-crossings in (nD)Cs at two-step laser excitation: Experiment and theory*, Optics Communications 264, 333–341 (2006).

[dis3] Marcis Auzinsh, Kaspars Blushs, Ruvin Ferber, Florian Gahbauer, **Andrey Jarmola**, and Maris Tamanis, *Electric-Field-Induced Symmetry Breaking of Angular Momentum Distribution in Atoms*, Physical Review Letters **97,** 043002 (2006)

[dis4] M. Auzinsh, K. Blush, R. Ferber, F. Gahbauer, **A. Jarmola**, M. S. Safronova, U. I. Safronova, and M. Tamanis, *Level Crossing Spectroscopy of the 7, 9, and 10$D_{5/2}$ states of ^{133}Cs and validation of relativistic many-body calculations of the polarizabilities and hyperfine constants*, Physical Review A 75, 022502 (2007).

[dis5] M. Auzinsh, K. Blushs, R. Ferber, F. Gahbauer, **A. Jarmola**, and M. Tamanis, *Level-crossing spectroscopy of the 7, 9, and 10D states of Cs in an external electric field*, Proceedings of SPIE Vol. 6604, 66040F-1-5 (2007).

Conferences

The results of this work have been reported in a number of international conferences and presented in the following conference abstracts:

- R. Ferber, M. Tamanis, **A. Jarmola**, E.A. Pazyuk, A.V. Stolyarov, *High resolution near-infrared diode laser spectroscopy of NaRb*, The 17th Colloquium on High Resolution Molecular Spectroscopy (Nijmegen, The Netherlands, September 9 – 13, 2001), p. 79.
- J. Alnis. M. Auzinsh, O. Docenko, **A. Jarmola**, M. Tamanis and R. Ferber, *Experiments on Electric Field Testing by Cs Atoms,* International workshop on Non-destructive electric field imaging and high-frequency plasma applications for nanoscale surface treatment, (Riga, Latvia, August 21 - 22, 2003), p. 20-21.
- J. Alnis. M. Auzinsh, O. Docenko, **A. Jarmola**, M. Tamanis, R. Ferber, *Cesium atomic vapour as tracer gas for optical imaging of electric field*, 1st International Meeting on Applied Physics (Badajoz, Spain, October 13 - 18, 2003), p. 100.

- **A. Jarmola,** J. Alnis. M. Auzinsh, O. Docenko, M. Tamanis and R. Ferber, *Electric field induced coherence destruction signals from the* $(7,9)^2D_{3/2}$ *levels of* ^{133}Cs, ECAMP 8 conference, (Rennes, France, July 6 - 10, 2004), vol. 2, p. 84.
- **A. Jarmola,** J. Alnis. M. Auzinsh, O. Docenko, M. Tamanis and R. Ferber, *Atomic vapour as tracer gas for optical imaging of sub-micro scale spatial distribution of electric field*, 7th International Conference on Nanostructured Materials, (Wiesbaden, Germany, June 20 - 24, 2004), p. 33.
- **A. Jarmola**, M. Auzinsh, K. Blushs, R. Ferber, F. Gahbauer and M. Tamanis, *Applications of Cesium Vapour as a Tracer Gas for Optical Imaging of Electric Fields*, International student conference on Development in Optics and Photonics (Riga, Latvia, April 30 – May 1, 2005), p. 34.
- M. Auzinsh, K. Blushs, R. Ferber, F. Gahbauer, **A. Jarmola**, and M. Tamanis, *Electric Field Induced Level Crossing Resonances and Alignment-orientation Conversion in* $nD_{3/2}$ *Cs Atoms,* International conference on Lasers and Optics in Atomic, Molecular and Nanoscale Physics, (Riga, Latvia, June 9 - 11, 2005), p. 4.
- M. Auzinsh, K. Blushs, R. Ferber, F. Gahbauer, **A. Jarmola**, and M. Tamanis, *Observation Of Stark Level Crossing Signals in* $7^2D_{3/2}$ *Cs Applying Two-Step Diode Laser Excitation,* 5th International Conference on Tunable Diode Laser Spectroscopy, (Florence, Italy, July 11 - 15, 2005), p. 101.
- M. Auzinsh, K. Blushs, R. Ferber, F. Gahbauer, **A. Jarmola**, and M. Tamanis, *Electric Field Induced Alignment - Orientation Conversion in Cs Atoms at Diode Laser Excitation,* 5th International Conference on Tunable Diode Laser Spectroscopy, (Florence, Italy, July 11 - 15, 2005), p. 172.
- M. Auzinsh, K. Blushs, R. Ferber, F. Gahbauer, **A. Jarmola** and M. Tamanis, *Stark level crossing signals in 7, 9,* $10^2D_{3/2}$ *Cs at two-step laser excitation,* 37th EGAS Conference (Dublin, Ireland, August 3 - 6, 2005), p. 127.
- M. Auzinsh, K. Blushs, R. Ferber, F. Gahbauer, **A. Jarmola** and M. Tamanis, *Observation of alignment-to-orientation conversion in the presence of an external electric field,* 37th EGAS Conference (Dublin, Ireland, August 3 - 6, 2005), p. 151.
- M. Auzinsh, K. Blushs, R. Ferber, F. Gahbauer, **A. Jarmola** and M. Tamanis, *Electric field induced Zeeman sublevel crossing resonances within hyperfine (nD)-manifold in cesium vapour*, 2nd Latvian Conference "Functional Materials and nanotechnologies" (Riga, Latvia, March 27 - 28, 2006), p. 8.

- M. Auzinsh, K. Blushs, R. Ferber, F. Gahbauer, **A. Jarmola** and M. Tamanis, *Alignment to orientation conversion in Cs in a pure electric field: experiment theory and applications,* 38th EGAS Conference (Ischia, Italy, June 7 - 10, 2006), p. 102.
- M. Auzinsh, K. Blushs, R. Ferber, F. Gahbauer, **A. Jarmola** and M. Tamanis, *Electric field induced hyperfine level crossing signals in 7, 9, $10^2D_{5/2}$ Cs at two-step laser excitation,* 38th EGAS Conference (Ischia, Italy, June 7 - 10, 2006), p. 177.
- M. Auzinsh, K. Blushs, R. Ferber, F. Gahbauer, **A. Jarmola** and M. Tamanis, *Electric field induced level crossing resonances within hyperfine (nD)-manifold in cesium vapour,* Advanced Optical Materials and Devices (Vilnius, Lithuania, August 27 - 30, 2006), p. 24.
- M. Auzinsh, K. Blushs, R. Ferber, F. Gahbauer, **A. Jarmola** and M. Tamanis, *Level-crossing spectroscopy of the 7, 9, and 10D states of Cs in an external electric field*, 14th International School on Quantum Electronics "Laser Physics and Applications 2006" (Sunny Beach, Bulgaria, September 18 - 22, 2006), p. 63.
- M. Auzinsh, K. Blushs, R. Ferber, F. Gahbauer, **A. Jarmola** and M. Tamanis, *Coherent effects in nD Cs: level crossing spectroscopy and alignment-to-orientation conversion*, Advances in Laser Spectroscopy: in Memory of Prof. Maris Jansons 1936-1997 (Riga, Latvia, September 28 - 29, 2006), p. 15.
- M. Auzinsh, K. Bluss, R. Ferber, F. Gahbauer, **A. Jarmola**, M. S. Safronova, U. I. Safronova, and M. Tamanis, *Hyperfine structure constants of the 7, 9, $10D_{5/2}$ states of cesium*, ECAMP9 Conference, (Crete, Greece, May 6 – 11, 2007), p. Th2-6
- M. Auzinsh, K. Bluss, R. Ferber, F. Gahbauer, **A. Jarmola**, M. S. Safronova, U. I. Safronova, and M. Tamanis, *Coherent effects in Cs (nD) states in the presence of an external electric field*, CLEO/Europe-IQEC 2007 conference, (Munich, Germany, June 17 - 22, 2007), p. 110.
- M. Auzinsh, K. Blushs, R. Ferber, F. Gahbauer, **A. Jarmola** and M. Tamanis, *Optical Non-Contact Electric Field Mapping by LIF in Cs vapor,* Frontiers in Optics 2007, Laser Science XXIII conference, (San Jose, California, USA, September 16 – 20, 2007)

2. Electric-field-induced level-crossings spectroscopy in Cs atoms

2.1 Level-crossing method

The level-crossing method is one of the simplest and most effective spectroscopic methods for investigating the structures of atomic levels. Level-crossing spectroscopy works by measuring changes in the spatial intensity distribution or the polarization characteristics of fluorescence that is emitted from coherently excited levels that take place when these levels cross under the influence of external magnetic or electric fields.

Compared with other Doppler-free techniques, level-crossing spectroscopy has some definite experimental advantages: experimental arrangements are relatively simple; narrow-line laser excitation is not needed, experiments can be performed in a simple vapour cell without collimated atomic beams. The main disadvantage of this method is that the absorption profile changes with external field. The laser bandwidth should be sufficiently large to excite all magnetic sublevels independent of the field strength.

Electric-field-induced level-crossing spectroscopy has not been exploited as extensively as magnetic-field-induced level-crossing spectroscopy to determine atomic properties, because a homogenous electric field is harder to produce and measure than a magnetic field which causes a comparable magnetic sublevel splitting.

The first experimental observation of electric-field-induced magnetic sublevel (m_F) crossing within a hyperfine manifold was reported in 1966 by A. Khadjavi et. al. [7]. In that work, the Stark effect was studied in the second excited states of the alkali atoms ^{85,87}Rb($6P_{3/2}$) and ^{133}Cs($7P_{3/2}$) populated by resonant radiation from a gas-discharge lamp. Resonance signals in the fluorescence light from the excited states have been observed when the electric field was scanned. The positions of the resonances corresponded to the level-crossing electric field values. This method has been applied by the same authors to determine the tensor polarizabilities a_2 for these states [8] and for ^{39}K($5P_{3/2}$) state [9].

In the present thesis [dis2, dis4] electric-field-induced level-crossing resonances of m_F magnetic sublevels within hyperfine levels F at two-step laser excitation have been studied experimentally and described theoretically for the first time. Tensor polarizabilities a_2 of the nD$_{3/2}$ states and hyperfine structure constants A of the nD$_{5/2}$ states of Cs with n = 7, 9, and 10 have been obtained.

2.2 Theory of Stark effect

The interaction of an atom and a static uniform electric field E is described by the operator:

$$V = -\mathsf{E} \cdot \mathbf{P} \ , \tag{2.1}$$

where $\mathbf{P} = e\sum_i \mathbf{r}_i$ is the electric dipole moment. Since **r** has nonzero matrix elements only between states of opposite parity, the average value of *V* in any parity eigenstate vanishes. Hence, the change in energy of a state *f*, to lowest order in E, is given by the second-order perturbation formula:

$$\Delta E(f) = \left\langle f \left| \sum_i \frac{\mathsf{E} \cdot \mathbf{P} |i\rangle\langle i| \mathsf{E} \cdot \mathbf{P}}{E(f) - E(i)} \right| f \right\rangle = \left\langle f \left| \mathsf{H}' \right| f \right\rangle \ , \tag{2.2}$$

where the sum extends over all intermediate states *i* of the atom. From (2.2) we see that energy shift can be regarded as the diagonal matrix element of the effective Hamiltonian operator H'. One can use the algebra of spherical tensors [8, 9] to show that for a state of electronic angular momentum *J* and for an electric field along the *z* axis, the effective Hamiltonian is:

$$\mathsf{H}' = -\frac{1}{2} a_0 \mathsf{E}_z^2 - \frac{1}{2} a_2 \mathsf{E}_z^2 \frac{3J_z^2 - J(J+1)}{J(2J-1)} \ , \tag{2.3}$$

where α_0 and α_2 are the scalar and tensor polarizabilities of the atom, respectively.

The effective Hamiltonian may be regarded as a first-order perturbation within the sublevels of the atomic state *J*. Since the atomic sublevels are also perturbed by the interaction $\mathsf{H}_{\rm hfs}$ between the atomic electrons and the nucleus, the energies and eigenstates of the atom are just the eigenvalues and eigenvectors of the Hamiltonian operator:

$$\mathsf{H} = \mathsf{H}_{hfs} + \mathsf{H}' \ . \tag{2.4}$$

The hyperfine interaction $\mathsf{H}_{\rm hfs}$ can be expressed to sufficient accuracy in terms of the magnetic dipole and electric quadrupole coupling constants *A* and *B*:

$$\mathsf{H}_{hfs} = A\mathbf{I} \cdot \mathbf{J} + B \frac{3(\mathbf{I} \cdot \mathbf{J})^2 + 3/2(\mathbf{I} \cdot \mathbf{J}) - I(I+1)J(J+1)}{2I(2I-1)J(2J-1)} \ . \tag{2.5}$$

In diagonalizing (2.4) one can ignore the scalar component of the effective Hamiltonian (2.3) since this simply shifts all energy levels of the atomic multiplet by the same amount.

2.3 The nD$_{3/2}$ states: tensor polarizability

2.3.1 Hyperfine level splitting of Cs nD$_{3/2}$ states in an external electric field

Cesium has only one naturally occurring stable isotope ^{133}Cs with nuclear spin I = 7/2. As a result of the hyperfine interaction, the Cs ground state level 6S$_{1/2}$ splits into two hyperfine structure (hfs) components with total angular momentum quantum numbers F_g = 3 and F_g = 4. The ground state hfs components are separated by approximately 9 GHz. The excited states nP$_{3/2}$ and nD$_{3/2}$ consist of four hfs components with F_e = 2, 3, 4, and 5. The separation between 6P$_{3/2}$ Cs state hfs components is of order several hundred MHz. The 7D$_{3/2}$ state hfs components are separated by several tens of MHz, but the 9 and 10D$_{3/2}$ states only by several MHz. When an electric field is applied, each hfs level F splits into F + 1 magnetic sublevels m_F, which can cross at certain electric field values.

To predict electric field values at which magnetic sublevels m_F of the hyperfine levels cross (resonance positions in the fluorescence) it is useful to calculate the energy level splitting diagram in an external electric field for the hfs levels of the nD states of Cs. Figure 2.1 shows such diagrams for the 7, 9, and 10D$_{3/2}$ states of Cs calculated by diagonalizing in an uncoupled basis the Hamiltonian (2.4), which includes the hyperfine and Stark interactions [38]. This Hamiltonian was computed the theoretical values of the tensor polarizability α_2 from the paper of Wijngaarden et al. [39] (see table 2.1) and the experimental values of the hfs constant A from the review paper of Arimondo et al. [40] A = 7.4(2) MHz for 7D$_{3/2}$ (measured in [40]), A = 2.35(4) MHz for 9D$_{3/2}$, and A = 1.51(2) MHz for 10D$_{3/2}$ (measured in [41, 42]). No information about the hfs constant B for this states exist in the literature and it assumed to be negligibly small due to the small quadrupole moment of Cs.

As can be seen from Fig. 2.1, two level crossings for the nD$_{3/2}$ states of Cs are predicted: one crossing within the F=4 manifold with $\Delta m_F = \pm 2$ and $\Delta m_F = \pm 1$ and a second between magnetic sublevels $m_F = \pm 3$ of the F=4 hfs level and $m_F = \pm 5$ of the F=5 hfs level. When linearly polarized light excites the atoms and linearly polarized fluorescence is observed, resonance signals in the fluorescence at electric field values corresponding to the level crossings with $\Delta m_F = \pm 2$ are expected.

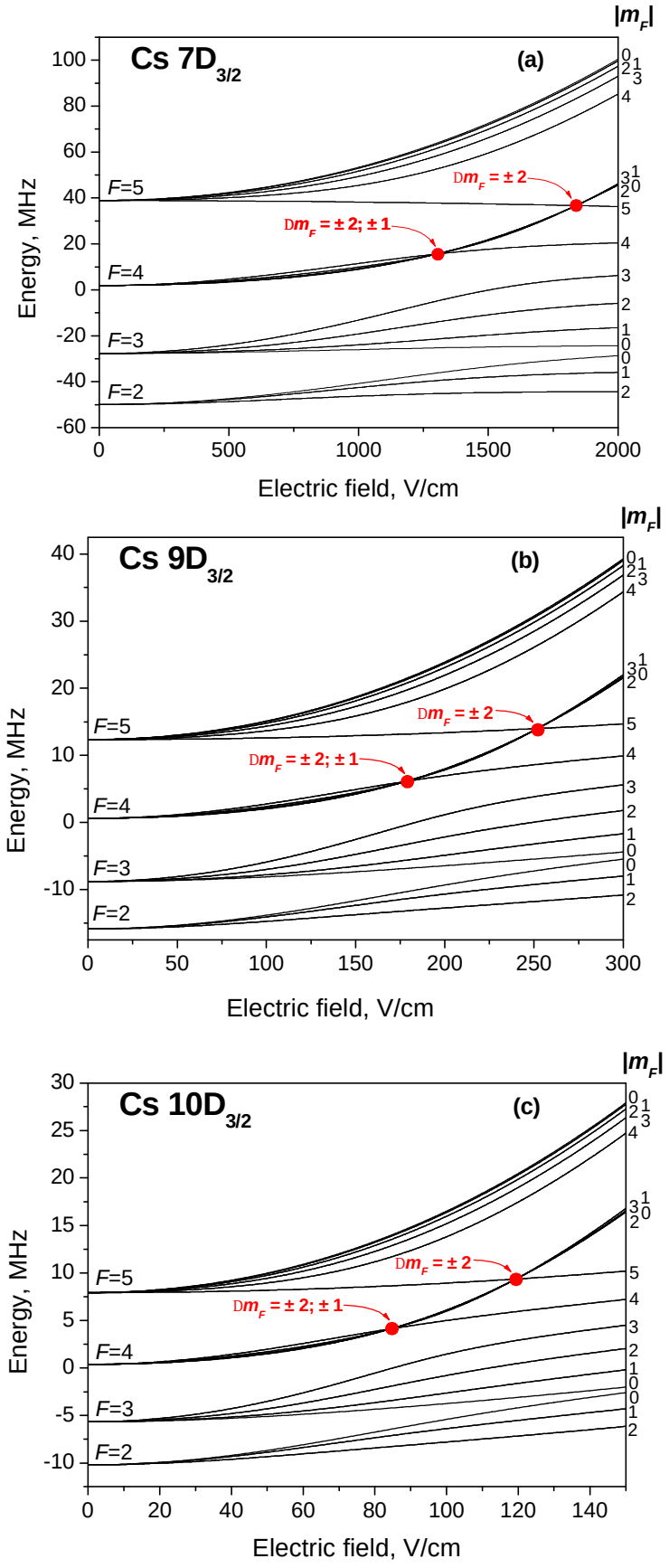

Fig. 2.1. Hyperfine level-splitting diagram in an external electric field for the (a) 7 $D_{3/2}$, (b) $9D_{3/2}$, and (c) $10D_{3/2}$ states of Cs.

2.3.2 Experimental setup

The measurements were made on cesium vapour contained in a sealed glass cell at room temperature. An electric field was produced by transparent Stark electrodes located inside the cell (see Fig. 2.2). The electrodes consist of two glass plates, on which indium-tin-oxide vapour had been deposited. The electrodes are separated by two ceramic spacer-rods with a diameter of 2.5 mm.

In order to populate the 7, 9, and $10D_{3/2}$ states of cesium from the ground state, two-step laser excitation was used (see Fig. 2.3). In the first step $6S_{1/2} \rightarrow 6P_{3/2}$, atoms were excited by the linearly polarized diode laser radiation (LD-0850-100sm laser diode) with polarization vector $\mathbf{E_1}$ parallel to the external electric field E direction ($\mathbf{E_1}||\mathsf{E}||\mathbf{z}$, see Fig. 2.4). In the second step, to induce the $6P_{3/2} \rightarrow nD_{3/2}$ transition, radiation from either a diode laser (Hitachi HL6738MG laser diode) for n = 7 or a Coherent CR699-21 ring dye laser with Rhodamine 6G for n = 9, 10 was used. Radiation from the second laser was sent in a counterpropagating direction and polarized such that $\mathbf{E_2}$ was perpendicular to the electric field E direction ($\mathbf{E_2}||\mathbf{y}$). The diameters of the laser beams in the interaction region were approximately 1 mm. To avoid optical pumping, neutral density filters were used. The power did not exceed 3mW for the diode lasers and 10mW for the dye laser. The experimental setup is shown on Fig. 2.5.

Fig. 2.2. Glass cell with an electrodes and a Cs vapour.

Both diode lasers were designed as external cavity diode lasers in the Littrow configuration. To stabilize the first diode laser, a Thorlabs temperature controller TEC 2000 and laser diode controller LDC 500 were used, while for the second diode laser self-made controllers based on Thorlabs circuit boards TCM1000T and LD1255 for the temperature and current control, respectively, were used. Typical operating laser diode temperature and current values were in the range 20 - 25 °C and 60 - 80 mA.

Since the absorption profile of atomic transitions changes with electric field, the linewidths of both lasers should be broad enough to ensure that all magnetic sublevel components absorb the radiation independent of the electric field strength. The broad linewidth provide a stable fluorescence signal from the excited nD state when two-step laser excitation is applied. At the same time the radiation of the first laser should be narrow enough

to resolve the two-ground state hfs components. In order to populate most efficiently those hfs components of the final nD$_{3/2}$ state that contain level crossings (F_f = 4, F_f = 5) and to avoid or reduce the excitation of the hfs components that contain no level crossings and thus contribute only background, the atoms where excited from the F_g = 4 hfs component of the ground state.

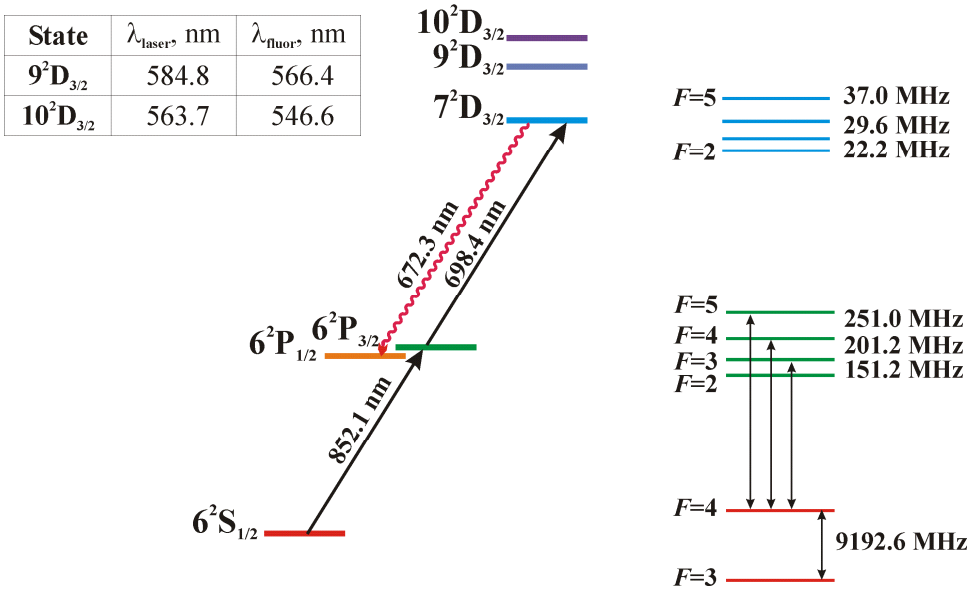

Fig. 2.3. Cesium energy levels and excitation-observation scheme for the nD$_{3/2}$ states.

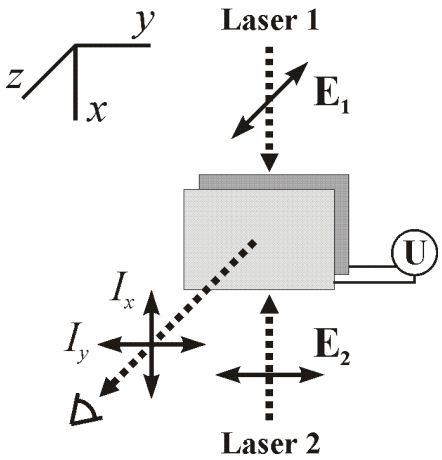

Fig. 2.4. Experimental geometry.

The line-width of our external cavity diode lasers is of order 10-20 MHz, which is too small to excite all magnetic sublevel components simultaneously. Nevertheless, it has been found that at some operating regimes for the first-step diode laser, the overall resonance fluorescence intensity as observed by a CCD camera is more stable in time. By investigating the diode laser line profile at that operating regime with a TROPEL Model 240 spectrum analyser with 7.5 GHz free spectral range, two symmetrical broad (approx 1GHz) sidebands appear in the laser output spectrum in addition to the narrow central line. This broad sideband

laser excitation was used to obtain a more stable signal. In order to broaden the second laser linewidth its frequency was jittered over a spectral range of 1GHz by applying a saw-tooth signal of tens Hz to the piezo-electric crystal mounted on its grating.

When high voltage was applied to the electrodes, then electric current was observed to flow. It happens because of a thin cesium layer which condenses on the electrodes and ceramic spacer-rods. In order to avoid this condensation, the cell was placed in an oven and kept at a temperature around the melting point of Cs (28 °C) a few degrees above room temperature.

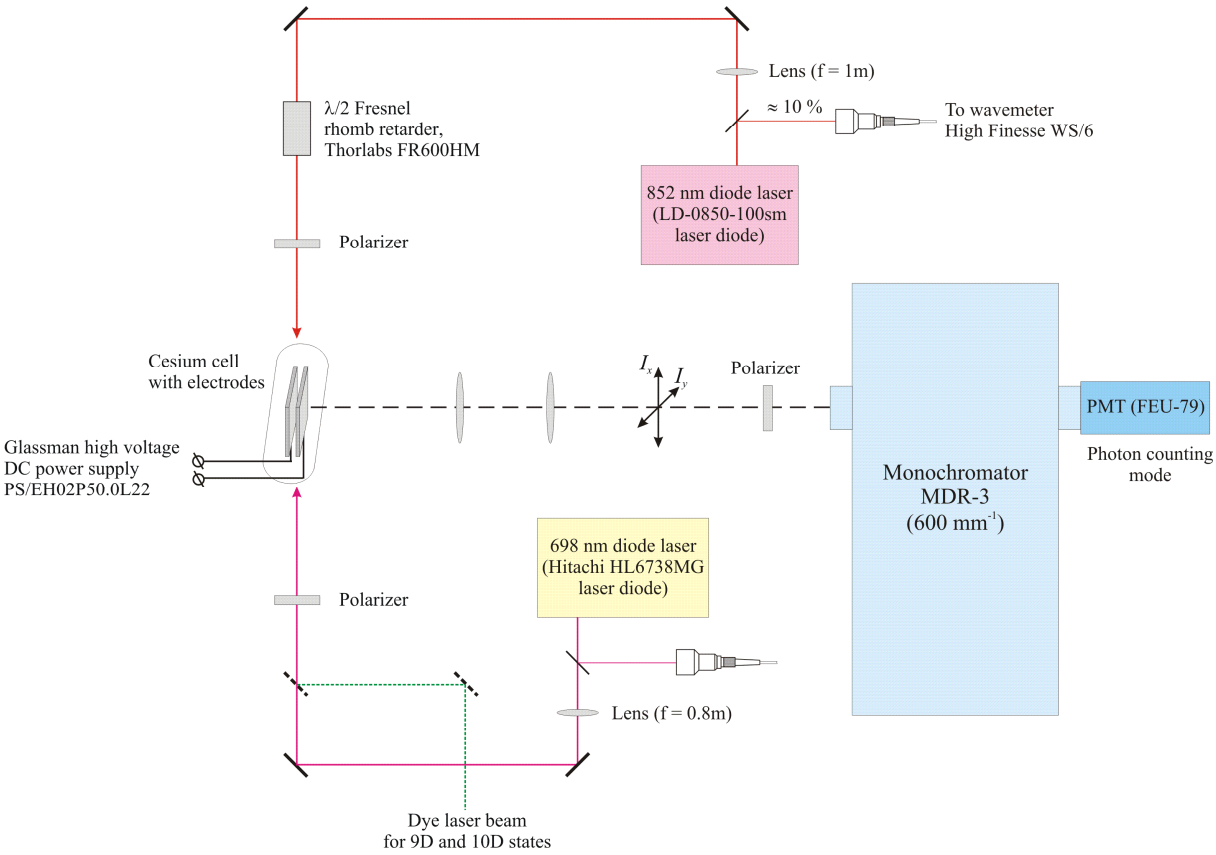

Fig. 2.5. Experimental setup.

The laser induced fluorescence (LIF) from the nD$_{3/2}$ states to the 6P$_{1/2}$ state was observed along the electric field direction. The dependence on the electric field strength of the LIF intensity components I_x and I_y (which are polarized perpendicular and parallel to $\mathbf{E}_2$, respectively, (see Fig. 2.4) was studied. The LIF was focused onto the entrance slit of the MDR-3 monochromator by a two lens system. The signal was detected by a photomultiplier tube FEU-79 which operated in photon counting regime. During the experiment the voltage between the electrodes was scanned continuously a scan period of approximately 200 s. The photon counts were accumulated during 1 second intervals and recorded together with

electrode voltage values on a PC. The dependence of the fluorescence intensity on the electric field values shown in Fig. 2.6 – 2.8 represents an averaged experimental signals over a few tens of scans.

2.3.3 Results

The level-crossing signals for the $7D_{3/2}$, $9D_{3/2}$, and $10D_{3/2}$ states of Cs are shown in Figures 2.6 and 2.7, where the LIF relative intensity is plotted as a function of the electric field strength. Experimentally measured signals are represented by dots and simulations by solid lines. Simulations are based on a theoretical model developed and described in details in [dis2]. Signals for two different experimental geometries labelled as *zyx* and *zyy* are presented, where the first and the second letters *z* and *y* denote the orientation of the polarization of the first and second lasers, $\mathbf{E}_1 \| z$ and $\mathbf{E}_2 \| y$, and the third letter, *x* or *y* denotes the polarization direction of the observed LIF (see Fig. 2.4).

The level-crossing signals for the nD$_{3/2}$ states contain two well pronounced resonances. The positions of these resonances correspond to the electric field values at which magnetic sublevels with $\Delta m_F = \pm 2$ cross (see Fig. 2.1). The level-crossing positions depend on the values of the tensor polarizability a_2, and the hfs constant A of the atomic state (the hfs constant B for the nD states of Cs have been reported to be negligibly small [40]). Thus by measuring the resonance position it is possible to determine either tensor polarizability a_2 or hfs constant A, assuming that one of them is known. The hfs constant A values for the nD$_{3/2}$ states of Cs are known sufficiently well, which allows one to measure the tensor polarizabilities a_2 of these states.

The electric field between the electrodes can be measured by measuring the voltage applied on the electrodes and the spacing between them. The main contribution to the uncertainty of the electric field measurements is the uncertainty of the measurement of the electrodes spacing. In the present experiment, however, it was possible to calibrate the electric field between the electrodes with high precision by comparing an experimentally measured resonance position with the calculated one for the $10D_{3/2}$ state of Cs (see Fig. 2.7b). The experimental value of the tensor polarizability a_2 for the $10D_{3/2}$ state is known with unprecedented accuracy $a_2 = 3.4012(36)\times 10^6\ a_0^3$ [43] and together with the hfs constant A = 1.51(2) MHz could be used to calculate a theoretical curve. By comparing the position of the resonance peak of the measured curve at approximately 120 V/cm with the calculated position, it was found that electric field scale should be corrected by 2 %. This illustrates the precision with which we knew the electrode spacing before calibration.

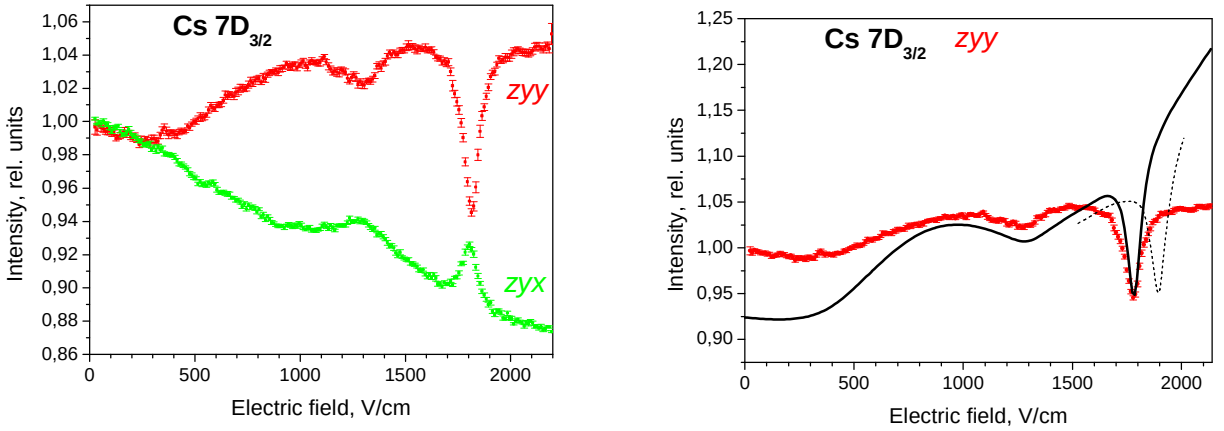

(a) (b)

Fig. 2.6. Fluorescence vs. electric field strength for the $7D_{3/2}$ state of Cs, (a) experimental results for the *zyy* and *zyx* geometry, (b) experiment and theory for the *zyy* geometry. Dots - measurements, solid line - calculations, dashed line - calculations using the tensor polarizability value from [44].

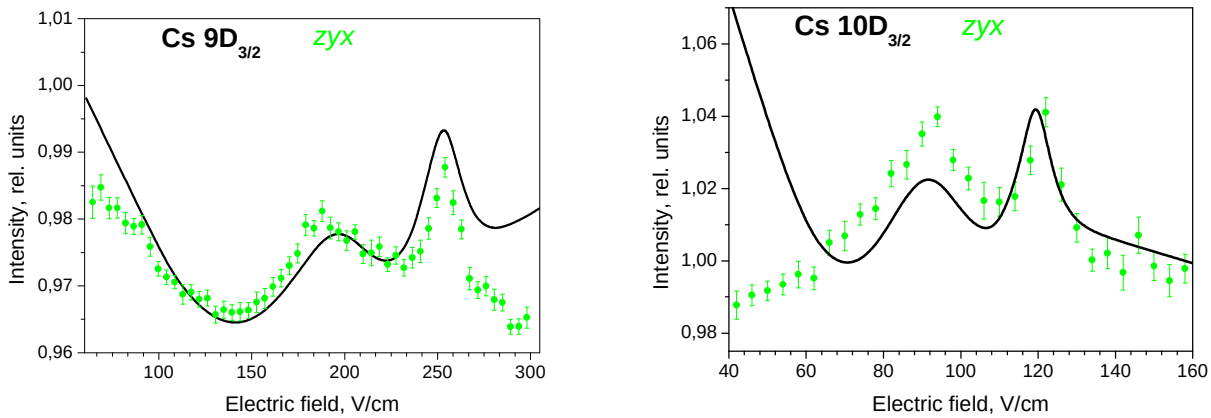

(a) (b)

Fig. 2.7. Fluorescence vs. electric field strength for the (a) $9D_{3/2}$ and (b) $10D_{3/2}$ state of Cs, *zyx* geometry. Dots - measurements, solid line – calculations. Electric field scale for the $10D_{3/2}$ state before calibration is plotted.

The electric field scales in Fig. 2.6 and 2.7(a) for the $7D_{3/2}$ and $9D_{3/2}$ state level-crossing signals are adjusted using the scaling factor obtained from the calibration with the $10D_{3/2}$ state level-crossing signal. The theoretical curve was calculated using hyperfine constants A from [40], and the tensor polarizabilities a_2 have been adjusted so that level-crossing resonance positions agree with the experimental ones. To illustrate the sensitivity of the method in Fig. 2.6(b) the results of the calculations of the level-crossing resonance position using the previously measured a_2 value [44] (dashed line) have been included. The results of a_2 measurements for the $7D_{3/2}$ and $9D_{3/2}$ states are given in Table 2.1 and compared

with previous measurements and theoretical calculations. The measured tensor polarizability value for the $9D_{3/2}$ state agreed within experimental error with previously measured and calculated values. However, the presently measured a_2 value for the $7D_{3/2}$ state differs from the previously measured value by approximately 15 %.

The largest contributions to the uncertainty of the tensor polarizability a_2 value are from the uncertainty in the hfs constants A of the states under study and in the electric field calibration. The accuracy of the present measurements is slightly higher than that reported from the previous experiments for the same atomic states (see Table 2.1).

Table 2.1. Comparison of the experimentally obtained tensor polarizabilities with previous experiments and theory.

Cesium atomic state	Hyperfine constant (MHz)	Tensor polarizability α_2 (a_0^3)		
		This experiment	Previous experiment	Theory
$10D_{3/2}$	1.51(2) [40]	-	$3.4012(36) \times 10^6$ [43]	3.41×10^6 [39]
$9D_{3/2}$	2.35(4) [40]	**$1.183(35) \times 10^6$**	$1.258(60) \times 10^6$ [45]	1.19×10^6 [39]
$7D_{3/2}$	7.4(2) [40]	**$7.45(20) \times 10^4$**	$6.6(3) \times 10^4$ [44]	7.04×10^4 [39]

The disagreement between the calculations and the experimental signals at electric field values far above and below the level crossing positions can be explained as follows. The shape of the calculated level-crossing signals is very sensitive to various parameters, such as both lasers radiation intensities, spectral widths, and wavelength detuning from the exact atomic transitions which were not possible to control precisely in the present experiment. To calculate the curve which describes accurately the experimental signal it is necessary to adjust these parameters in the calculations, but calculations which involve so many parameters are extremely time consuming. However, the position of the level-crossing resonances does not depend on these parameters (the ac Stark effect is negligibly small at the laser powers used), but depend only on the atomic constants α_2 and A. In order to obtain accurate tensor polarizability α_2 values it is sufficient to use calculations which describe well the experimental signal only in the vicinity of level-crossing resonances. In the case of Cs nD$_{5/2}$ states well resolved resonances could no longer be observed, and an accurate theoretical description of the experimental signal in whole range becomes essential to obtaining reliable atomic constant values (see chapter 2.4.).

The parameter which is the most difficult to control during the experiment and which produces the most significant changes in the level-crossing signal is the laser wavelength detuning. Figure 2.8 illustrates the dependence of the experimentally obtained level-crossing signal on the second-step laser (dye laser) wavelength detuning for the $10D_{3/2}$ state of Cs. The overall changes of the signal do not change the level-crossing resonance position.

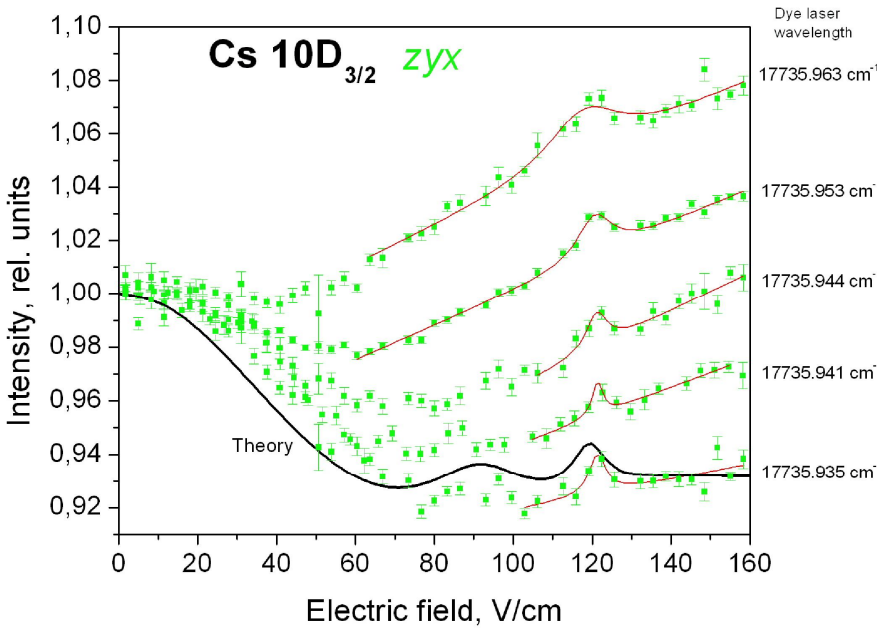

Fig. 2.8. Level-crossing signal of the $10D_{3/2}$ state of Cs dependence on the laser wavelength detuning. Electric field scale is not calibrated.

2.3.4 Conclusions

- Electric-field-induced level-crossing signals of m_F magnetic sublevels of the hyperfine F levels have been observed for the first time in two-step laser excitation.
- Experimentally obtained level-crossing signals for the 7, 9, and $10D_{3/2}$ states of cesium are described theoretically using correlation analysis of the optical Bloch equations in the case when an atom simultaneously interacts with two laser fields in the presence of an external electric field.
- New values of the tensor polarizabilities for the 7 $D_{3/2}$ and $9D_{3/2}$ states of Cs are determined from the level-crossing signals using an electric field calibration based on measurements of the $10D_{3/2}$ state.

2.4 The nD$_{5/2}$ states: hyperfine structure constants

2.4.1 Hyperfine level splitting of Cs nD$_{5/2}$ states in an external electric field

The nD$_{5/2}$ states of cesium consist of six hyperfine components with total angular momentum quantum numbers F_f = 1, 2, 3, 4, 5, and 6. The separation between these components for the 7, 9, and 10D$_{5/2}$ states is of order a few MHz. When an external dc electric field is applied each hyperfine component F splits into F +1 magnetic sublevels m_F (see Fig. 2.9). To calculate the hyperfine level-splitting diagrams in an external electric field shown on Fig. 2.9, the following experimental values of the tensor polarizability α_2 and hfs constant A have been used: α_2 = 1.29(4)×10^5 a_0^3 [44] and A = -1.7(2) MHz [40] for 7D$_{5/2}$, α_2 = 2.65(14)×10^6a_0^3 [45] and A = -0.45(10) MHz [40] for 9D$_{5/2}$, α_2 = 6.8148(197)×10^6 a_0^3 [43] and A = -0.35(10) MHz [40] for 10D$_{5/2}$. Unlike the case of nD$_{3/2}$ states, where there are only two well separated Δm_F = ±2 magnetic sublevel crossings (Fig. 2.1), and as a result well-pronounced level-crossing resonances are observed, the nD$_{5/2}$ states have seven closely spaced Δm_F = ±2 magnetic sublevel crossings. Therefore, nD$_{5/2}$ the level-crossing signals are overlapping and discernable resonances could no longer be observed.

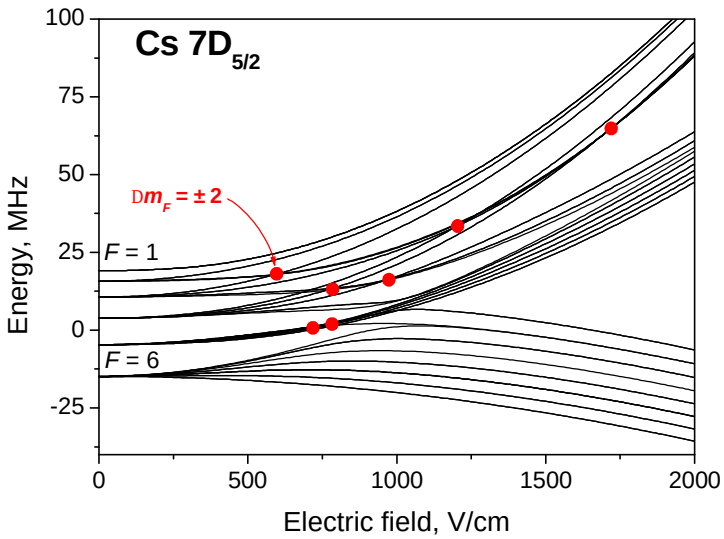

(a)

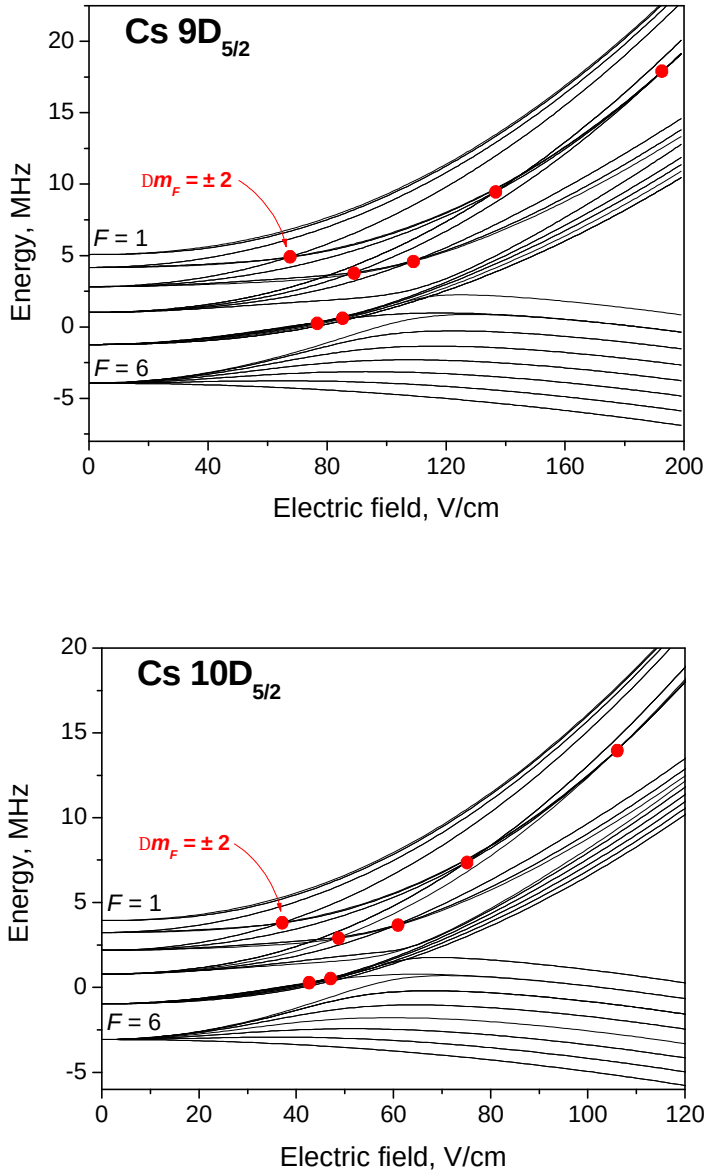

Fig. 2.9. Hyperfine level-splitting diagram in an external electric field for the (a) 7 $D_{5/2}$, (b) $9D_{5/2}$, and (c) $10D_{5/2}$ states of Cs. Circled points indicate level crossings with $\Delta m_F = \pm 2$.

2.4.2 Experimental set-up

The set-up of the nD$_{5/2}$ states level-crossing experiment is essentially the same as for nD$_{3/2}$ states (see chapter 2.3.2) except the one fact, which brings a small complication to the experiment. Namely, after two-step laser excitation $6S_{1/2} \rightarrow 6P_{3/2} \rightarrow nD_{5/2}$, the laser induced fluorescence (LIF) from the excited nD$_{5/2}$ states directly back to the $6P_{3/2}$ state should be observed (see Fig. 2.10). Since the observed LIF has the same wavelength as the second laser it is necessary to suppress the scattered light from the laser. This suppression was accomplished by means of diaphragms and careful alignment of the cell with respect to laser beams in order to reduce reflection from the electrodes. After final adjustments the

contribution of the scattered light to the signal was between 30% and 50%. It was checked that this background remains stable during the measurements and could be subtracted from the signal.

In order to avoid population of the final nD$_{5/2}$ state hfs component F_f = 6, which contains no level crossings (see Fig. 2.9) and thus would contribute only background, the atoms were excited from the ground state F_g = 3 hyperfine component (see Fig. 2.10). The electric field produced in the cell was calibrated using level-crossing signals for the 10D$_{3/2}$ state of Cs (see chapter 2.3.3).

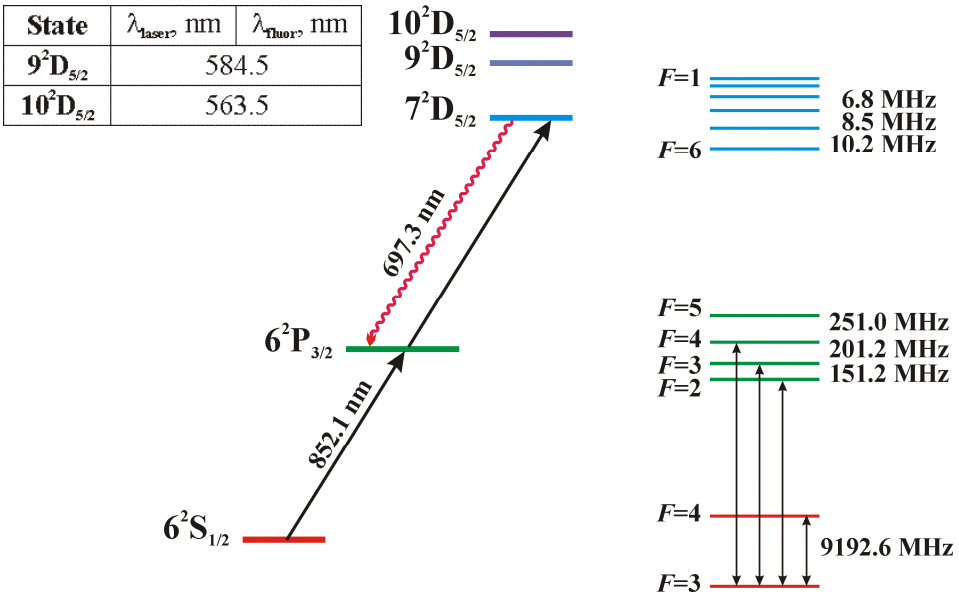

Fig. 2.10. Cesium energy levels and excitation-observation scheme for the nD$_{5/2}$ states.

2.4.3 Results

Level-crossing signals for the nD$_{5/2}$ states of cesium are plotted in Figs. 2.11-2.13, which present the dependence of the relative LIF intensity on electric field strength. Experimentally measured signals are represented by dots and simulations by solid lines. Simulations are based on a theoretical model developed and described in [dis2]. Signals for two different experimental geometries *zyy* and *zyx* are presented. As can be seen from Fig. 2.11-2.13, the obtained signals do not contain well pronounced level-crossing resonances as in case of the nD$_{3/2}$ states (see Fig. 2.6, 2.7). Nevertheless, atomic constant values could be obtained by fitting experimental data with the results of simulations based on a detailed theoretical model.

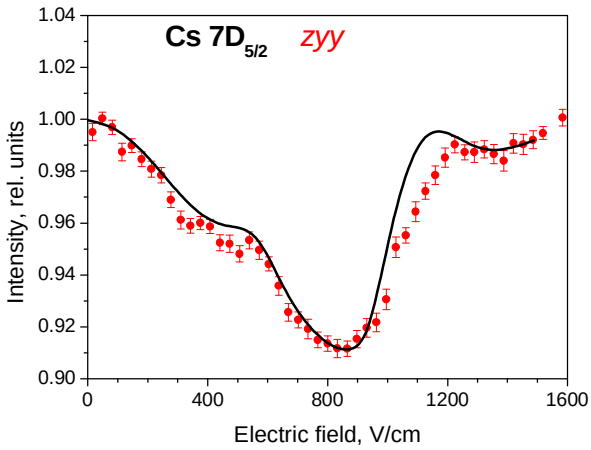

Fig. 2.11. Fluorescence vs. electric field strength for the $7D_{5/2}$ state of Cs, *zyy* geometry. Dots - measurements, solid line – calculations.

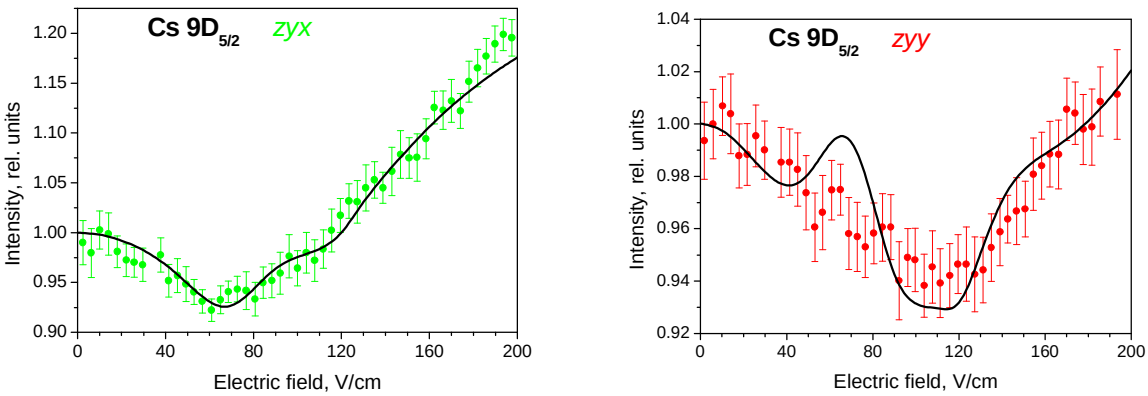

Fig. 2.12. Fluorescence vs. electric field strength for the $9D_{5/2}$ state of Cs, *zyx* and *zyy* geometry. Dots - measurements, solid line – calculations.

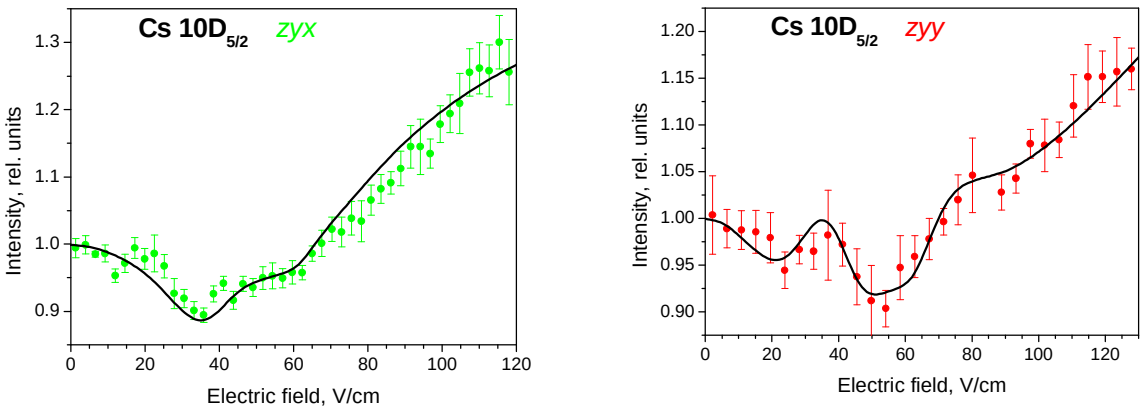

Fig. 2.13. Fluorescence vs. electric field strength for the $10D_{5/2}$ state of Cs, *zyx* and *zyy* geometry. Dots - measurements, solid line – calculations.

The obtained level-crossing signals depend on two atomic constants simultaneously: the tensor polarizability α_2 and the hfs constant A. If one of these constants is known, the experiment provides a way to determine the other. In the case of the $nD_{5/2}$ states, the level-crossing signals cannot be used to improve the knowledge of the tensor polarizabilities α_2, because the existing experimental values of the hfs constants contain uncertainties of the order of 30% [40]. The small hyperfine interaction makes them difficult to measure. At the same time, the experimental values of the tensor polarizabilities for the 7, 9, and 10 $D_{5/2}$ states are known with a much better precision (see Apendix A). The situation with the electronic structure calculations is similar to the experimental situation. The tensor polarizabilities α_2 can be calculated with far greater precision than the hfs constants. The accuracy of the α_2 calculations could be demonstrated by the excellent agreement of the calculations from [39] with very accurate experimental data for (10-13)$D_{3/2,5/2}$ states of Cs [43]. The estimates of the hfs constants are poor and hardly can be evaluated reliably. Therefore there is a need for more accurate values for the hfs constants of the $nD_{5/2}$ states.

In order to determine hfs constants the following approach has been used:

Ø Reliable theoretical values of the tensor polarizabilities α_2 have been obtained by performing all-order relativistic many-body calculations (the calculations were performed by M. S. Safronova from University of Delaware and U. I. Safronova from University of Nevada and could be found in [dis4]).

Ø The experimentally obtained signals were fitted with the results of simulations based on a theoretical model developed and tested in [dis2]. By fixing in the simulations the tensor polarizability α_2 at the calculated values, the fit of the level-crossing signals (see Figs. 2.11.-2.13) yields the values of the hfs constants A.

Table 2.2 summarizes the calculated tensor polarizabilities α_2 used in the simulations and the hfs constant values A obtained from the fit of the level-crossing signals. Measured values are compared with the previously measured values and with the values obtained from all-order relativistic many-body calculations [dis4]. The new obtained values of the hfs constants agreed with previously measured ones, but achieved greater precision. The results of the relativistic many-body calculation for the hfs constants A, considering the difficulty in calculating the hfs constants, agree reasonably well with the experimental measurements for the $7D_{5/2}$ and $9D_{5/2}$ states. However, the large discrepancy for the $10D_{5/2}$ state indicate that the calculations of the hfs constants cannot be considered reliable.

Table 2.2. Comparison of the experimentally obtained hyperfine constants with previous experiments and theory presented in [dis4].

Cesium atomic state	Calculated tensor polarizability α_2 (10^3 a_0^3)	Hyperfine constant (MHz)		
		This experiment	Previous experiment	Theory
$7D_{5/2}$	141.8(1.7)	**- 1.56(9)**	- 1.7(2) [40]	- 1.42
$9D_{5/2}$	2386(13)	**- 0.43(4)**	- 0.45(10) [40]	- 0.384
$10D_{5/2}$	6867(32)	**- 0.34(3)**	- 0.35(10) [40]	- 0.238

2.4.4 Conclusions

1. The pure electric field level-crossings of m_F magnetic sublevels of the hyperfine F levels have been studied experimentally and described theoretically for the nD$_{5/2}$ states of Cs with n = 7, 9, and 10.
2. New values of the hyperfine structure constants A for the 7, 9, and 10D$_{5/2}$ states of Cs are determined by means of measured level-crossing signals, a detailed theoretical description of these signals, and tensor polarizability values calculated with an all-order relativistic many-body method.

3. Alignment to orientation conversion in Cs atoms in the presence of an external electric field

3.1 Background

When atoms or molecules are excited by linearly polarized light, their angular momentum distribution in the excited state is symmetrical with respect to the polarization axis. In this situation the angular momentum of atoms or molecules is aligned. ***Alignment*** of the angular momentum means that magnetic sublevels $+m_J$ and $-m_J$ of the level J are populated equally while different $|m_J|$ sublevels are populated unequally. According to symmetry considerations, aligned atoms are able to produce only linearly polarized fluorescence and are not able to produce circularly polarized fluorescence.

However, under certain experimental conditions in the presence of external forces these strict symmetry rules can be broken, and excitation by linearly polarized light can produce an oriented ensemble of atoms. ***Orientation*** of the angular momentum means that magnetic sublevels $+m_J$ and $-m_J$ are populated unequally, which results in a circularly polarized fluorescence.

The anisotropic spatial distribution of angular momenta J could also be described by an atomic density matrix ρ [46]. An ensemble of particles is ***aligned*** if the distribution of angular momenta contains a net electric quadrupole moment or ***oriented*** if there is a net magnetic dipole moment. Orientation can be classified as *longitudinal* and *transverse*. Longitudinal orientation implies orientation along the direction of an external force. Transverse orientation means that orientation of atoms is perpendicular to the direction of an external force.

The breaking of the reflection symmetry of initially aligned atoms is called alignment to orientation conversion (AOC), which has been a subject of theoretical and experimental investigation since the 1960s, beginning with the work of [14-17]. The very first theoretical works suggested that AOC may be induced in atoms by a magnetic field gradient [14] or by anisotropic collisions in which the angle between the collision axis and the alignment axis differs from 0 and $\pi/2$ [15, 16]. These later predictions were experimentally observed by [47, 48]. Orthogonal static electric and magnetic fields were used to study AOC in Ba and Cs [49], while only a pure magnetic field was used to study AOC in Rb [50,51] and Na [52].

Electric-field-induced AOC was theoretically predicted and studied in detail in [19-21]. The only existing experimental observation of electric-field-induced AOC was performed in diatomic molecule NaK [53].

Electric-field-induced AOC can be understood classically as follows. An atom placed in an electric field E will become polarized, and, in general, the polarization will have a component parallel to the angular momentum J. This component leads to a torque on the angular momentum proportional to $(\mathsf{E}\cdot\mathbf{J})(\mathsf{E}\times\mathbf{J})$ that distorts the atomic angular momentum distribution in the plane perpendicular to the electric field and the axis of initial alignment [54]. Thus, initial alignment produced by linearly polarized light can be converted into transverse orientation when the aligned atoms are placed in a perturbing electric field that makes an angle with the initial alignment axis different from 0 or $\pi/2$, with the largest effect occurring at $\pi/4$. In the case of transverse orientation magnetic sublevels $+m_F$ and $-m_F$ are equally populated, but orientation results from coherent evolution of different hyperfine sublevels with $\Delta m_F = \pm 1$. A detailed theoretical treatment of the AOC in the external electric field could be found in [13].

The present study of AOC in the electric field was motivated as follows:

- AOC never had before been observed in atoms
- AOC can represent a potential background for electron electric dipole moment (EDM) searches in atomic or molecular systems. An understanding of this phenomenon will make it possible to take it into account as searches for an electron EDM become ever more sensitive.

In [dis3] the first experimental observations of AOC in atoms induced by an external electric field are reported.

3.2 The $n\mathrm{D}_{3/2}$ states: angular momentum distribution symmetry breaking [dis3]

3.2.1. Experimental setup

In the present experiment Cs vapour was produced in a sealed glass cell (Fig. 3.1) kept at room temperature. An electric field was applied via carefully polished stainless steel electrodes located inside the cell. The separation between electrodes was 5 mm, the diameter of the electrodes was 25 mm.

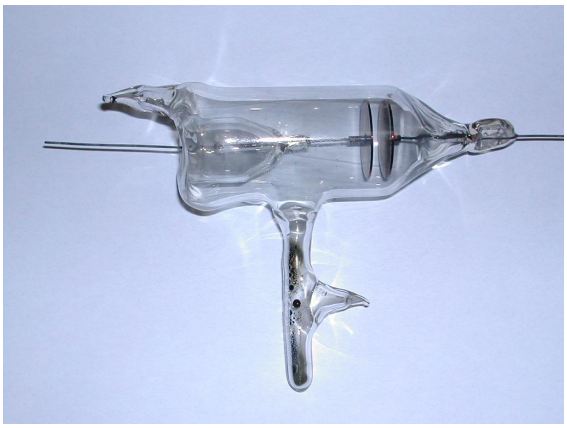

Fig. 3.1. Glass cell with metal electrodes and a Cs vapour.

The $7D_{3/2}$ and $9D_{3/2}$ states of Cs were populated by two-step laser excitation (see Fig.2.3). The laser setup was essentially the same as in level-crossing experiments (see chapter 2.3.2) with one exception for the second laser whose radiation $\mathbf{E_2}$ was polarized at an angle $\pi/4$ with respect to the first laser's radiation $\mathbf{E_1}$ and the electric field direction $\mathcal{E}$ (see Fig. 3.2).

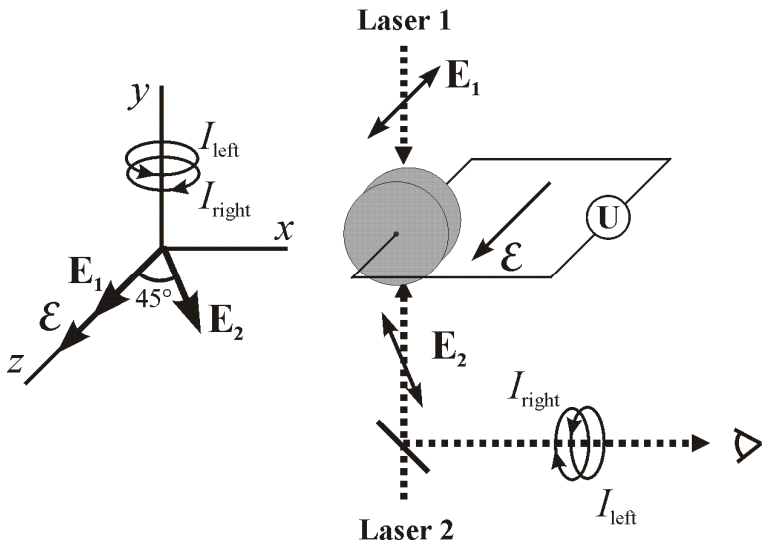

Fig. 3.2. Schematic diagram of the experiment. The electric field direction and the first laser polarization vector $\mathbf{E_1}$ are parallel to the z – axis. The second laser polarization vector $\mathbf{E_2}$ is directed at angle $\pi/4$ with respect to z - axis.

The laser induced fluorescence (LIF) from the excited $nD_{3/2}$ states to the $6P_{1/2}$ state was observed collinearly to the laser beams with the help of a pierced mirror. The LIF was focused onto the entrance slit of the MDR-3 monochromator by a two lens system. Before entering the monochronator, the LIF passed through a $\lambda/4$ plate which converts circularly polarized light into linearly polarized light, followed by polarizer whose polarization could be

switched between two orthogonal polarizations. In this way it was possible to measure the degree of circularity C defined as:

$$C = \frac{I(\mathbf{E}_{right}) - I(\mathbf{E}_{left})}{I(\mathbf{E}_{right}) + I(\mathbf{E}_{left})}\ , \tag{3.1}$$

where $I(\mathbf{E}_{\text{right}})$ and $I(\mathbf{E}_{\text{left}})$ are the intensities of the right and left circularly polarized light.

Interference filters were used in order to suppress scattered light from the second laser. The signal was detected by a FEU-79 photomultiplier tube operated in photon counting mode. The intensities of two orthogonally polarized fluorescence components were recorded on a personal computer together with the electrode voltage which was applied in discrete steps. The photon counts were accumulated during 1 second intervals for each polarization component while the electrode voltage was kept constant.

3.2.2 Results

The results of the measurements are presented as dots in Fig.3.4, where the degree of LIF circularity C for the 7 and $9D_{3/2}$ states is plotted as a function of the electric field strength. The degree of circularity reaches a maximum at the electric field value corresponding to the $\Delta m_F = \pm 1$ crossing (see Fig.2.1). The maximum values of C for the 7 and $9D_{3/2}$ states are 10% and 7.5%, respectively. A small orientation appears at zero electric field because the linewidth of the second laser is sufficiently broad to excite coherently magnetic sublevels that belong to different F states. This effect is more pronounced in the $9D_{3/2}$ state because of the smaller hyperfine level splittings.

The results of simulations are presented in Fig. 3.4 as solid lines. Simulations are based on a theoretical model developed and described in detail in [dis2]. The values of all parameters which have been used in the present simulations and which can not be measured precisely in the experiment are obtained by fitting simulations and measurements of the level-crossing signals of the same 7 and $9D_{3/2}$ states [dis2]. The level-crossing signals were obtained under the same experimental conditions. The parameters mentioned above include both laser's spectral widths and wavelength detuning from the exact atomic transitions. Tensor polarizability α_2 constant values measured in [dis2] and hyperfine structure constant values from [40] have been used in the simulations The excellent agreement between experiment and theory demonstrates the validity of the theoretical approach.

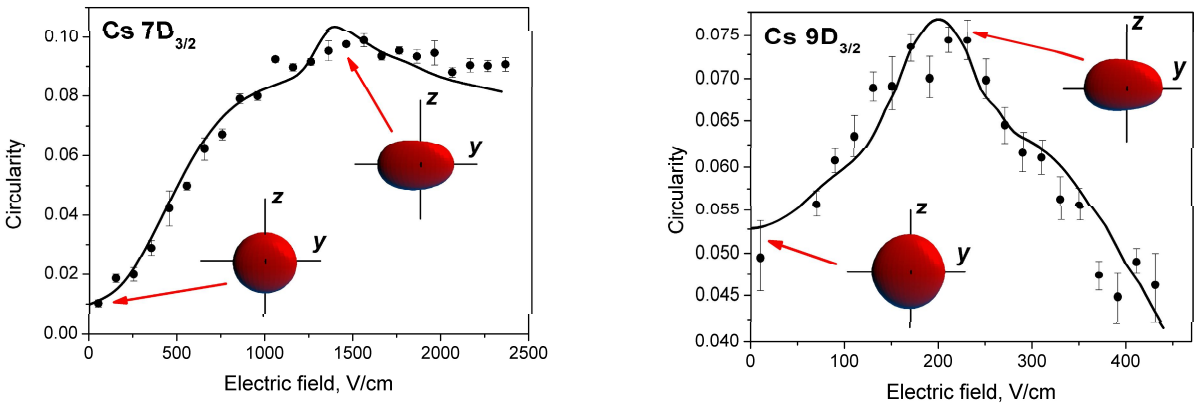

Fig. 3.4. Degree of LIF circularity *C* as a function of electric field for the $7D_{3/2}$ and $9D_{3/2}$ states of Cs. Dots: measurements. Solid line: calculations. Insets depict the atomic angular momentum distribution.

To convey an intuitive understanding of the AOC effect, Fig. 3.4 contains insets which help to visualize the angular momentum distributions at zero electric field and at the electric field value for which the degree of orientation was at maximum. The angular momentum distribution is visualized as a surface whose distance from the origin is proportional to the probability that the angular momentum of an atom in the ensemble points toward that point on the surface. This probability is computed from the components of the density matrix $r_{mm'}$ [21, 55].

3.2.3 Conclusions

- The alignment to orientation conversion signals induced by an external electric field have been observed for the first time in atoms, in the $7D_{3/2}$ and $9D_{3/2}$ states of Cs. When two-step laser excitation with polarization vector $\mathbf{E_1}$ parallel to the external electric field E and polarization vector $\mathbf{E_2}$ directed at angle $\pi/4$ with respect to E was applied, transverse orientation perpendicular to the $\mathbf{E}\mathsf{E}$ plane appeared, giving rise to LIF signals with a degree of circularity up to 10%.
- The experimentally obtained signals are described accurately by a detailed theoretical model based on correlation analysis of the optical Bloch equations.
- The phenomenon of AOC deforms distributions of atomic angular momentum in a manner that could mimic the signature of an electron electric dipole moment (EDM). Thus, AOC is a potential background for EDM searches in atomic or molecular systems. The present investigation shows that AOC can be understood very well and corrections could be made if necessary.

4. Optical imaging of an external electric field distribution

4.1 Electric field mapping methods

Electric field distribution imaging techniques have a long history and have only recently benefited from the use of lasers. Before the modern era, Langmuir probes [56] were used to map the electric potential rather than the field directly. A primary disadvantage of these probes was that they substantially perturbed the field to be measured. In the 1950s conducting surfaces in electrolytic tanks were used in the design of vacuum tubes in order to evaluate the fields of complicated geometries [57]. More recently, probes have been developed using the electro-optic (Pockels) effect [58, 59] and single-mode fiber interferometers [60]. These are never of high accuracy, but are useful in certain situations because they may be free of conducting materials.

Measurement of the Stark shift or Stark line broadening offers the possibility of mapping and calibrating electric fields both in plasmas and in vacuum. Spectral line broadening methods typically use the width of a given Rydberg level, such as in helium [61, 62], as a measure of the electric field. This method is clearly limited by other sources of line broadening, such as the Doppler effect and collisions. The actual displacement of Rydberg levels has been used to measure the electric field to about 1% in the cathode fall region of a Ne glow discharge [63].

It has been demonstrated by Harold Metcalf and co-workers [23] that the interference narrowing of Stark resonances could be used to measure an electric field to an unprecedented level of precision in a Rubidium atomic beam. Recently, new techniques for electric field imaging using large field-dependent coupling of the Rydberg states of Hg [64], and the dependence of laser induced fluorescence polarization on the electric field for the $B^1\Pi \rightarrow X^1\Sigma$ transition in the NaRb molecule [24] have been proposed.

In the present work, the possibility of using cesium vapour as a tracer gas to optically image electric field distributions has been studied. The presented technique is based on experimental and theoretical studies in [dis2-dis4] and takes advantage of the fact that the laser induced fluorescence intensity of the *n*D states of Cs depends on the external electric field strength.

4.2 Experimental set-up and results

A multifunctional stainless steel sample chamber was designed to facilitate allowing precise mounting and easy changing of test objects (see Fig. 4.1). The chamber has three glass windows. Laser beams transmitted through the windows W1 and W2 and optical signals are

observed with a CCD camera through the window W3. The chamber has simple connections to the vacuum system V and to the tracer gas supply G. The chamber was mounted on a 3D translation stage to allow precise positioning of testing objects.

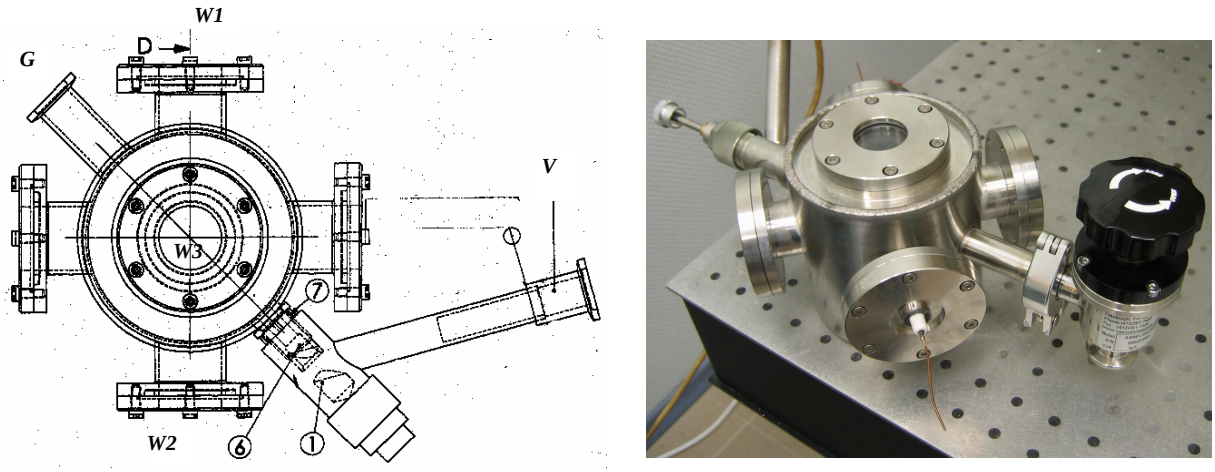

(a) **(b)**

Fig. 4.1. Multifunctional stainless steel sample chamber (a) sketch (top view), (b) photo

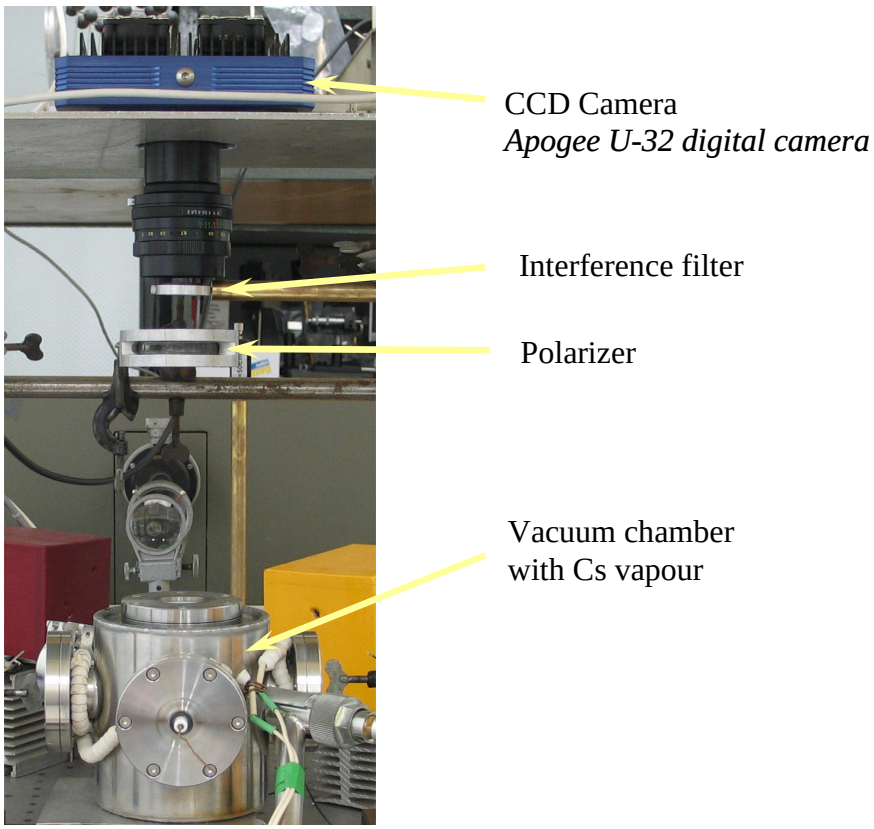

Fig. 4.2. Experimental set-up for the optical imaging of an external electric field distribution

Figure 4.2 shows the experimental set-up which has been used to demonstrate the possibility of using Cs vapour as a tracer gas to optically image electric field distributions. A series of experiments have been performed with two different testing objects. The first testing

object was a simple configuration of pin electrodes, where the distance between the pins and the grounded electrode was of the order of a few millimeters. The electrodes were placed in a chamber, and then the chamber was evacuated and filled with Cs vapour. The $7D_{3/2}$ state of cesium was populated by two-step laser excitation $6S_{1/2} \rightarrow 6P_{3/2} \rightarrow 7D_{3/2}$ (see Fig. 2.3) using two linearly polarized counter propagating diode laser beams. The laser induced fluorescence (LIF) was observed at the $7D_{3/2} \rightarrow 6P_{1/2}$ transition. The chamber was adjusted so that the laser beams propogated between the pin electrodes and grounded electrode. Before being detected by a CCD camera, the LIF passed through an interference filter (Thorlabs FB670-10) and a polarizer.

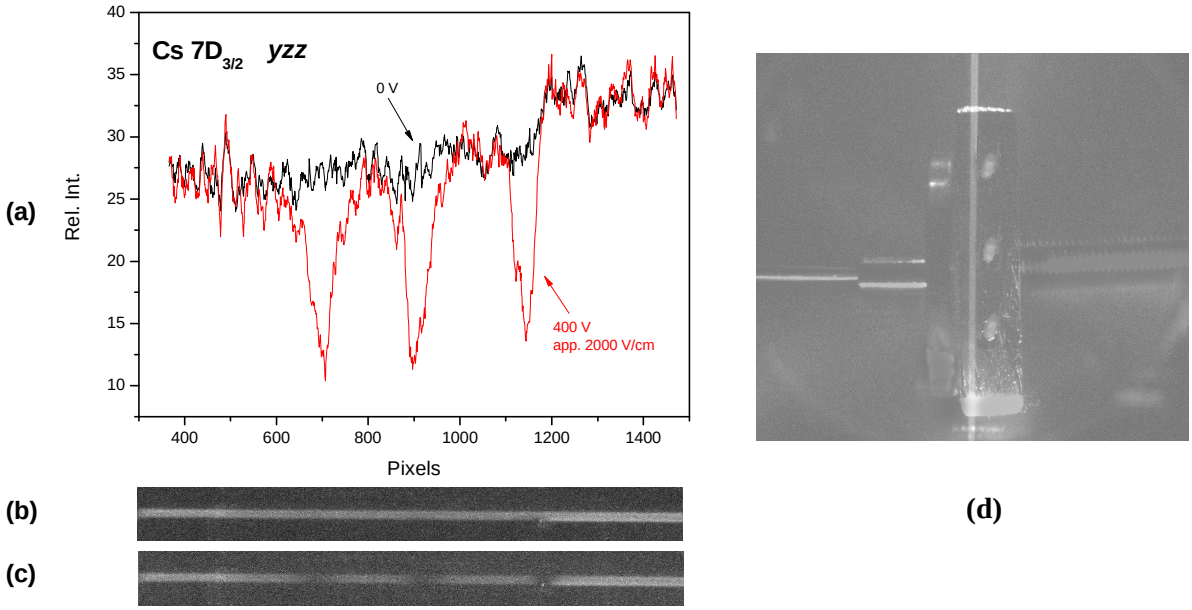

Fig. 4.3. Optical CCD-images of the effect of an electric field on the LIF intensities. Electric field distribution between electrodes along the laser beam are shown: (a) digitized output; (b) 400 V electric field; (c) zero electric field, (d) electrodes and laser induced fluorescence in Cs vapour.

The distribution of electric field was tested at different voltages applied between the electrodes. The results are presented in Fig. 4.3. From the LIF intensity distribution the position of all three pin electrodes could be clearly seen when electric field was applied. An applied electric field of order 2000 V/cm in the case of the $7D_{3/2}$ state causes changes in fluorescence intensity distribution of approximately 50 %.

The second testing object was designed and manufactured in collaboration with Baltic Scientific Instruments (BSI). This test object simulated a strip detector (a product of BSI) surface, see Fig. 4.4. The distance between strips for this electrode varied from 0.3 mm to 1 mm. It was also provided the option of keeping one of the strips at a potential, which differed from the other strips. Figure 4.5 shows a strip-type electrode placed inside the vacuum chamber.

The spatial resolution was greatly improved in this experiment by focusing the laser beams to a diameter at FWHM as small as to 90 μm. The experimental results are shown on Figs. 4.6 - 4.7.

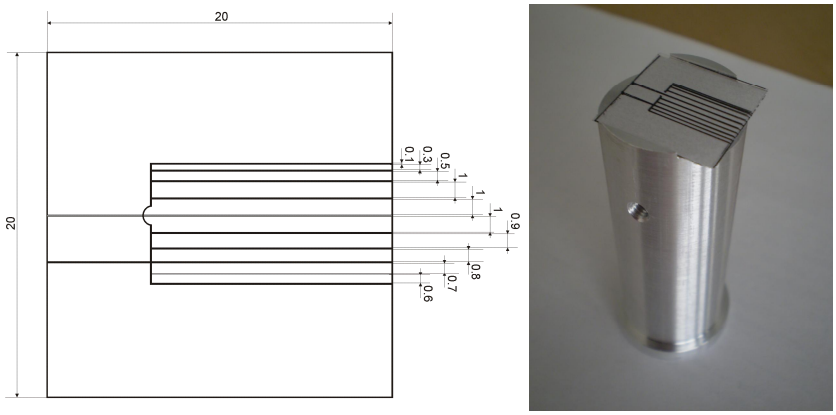

(a) **(b)**

Fig. 4.4. (a) Design of the electrode, which simulates the surface of a coplanar strip grid CdZnTe detector (a product of BSI); (b) Strip electrode detector open surface testing sample block.

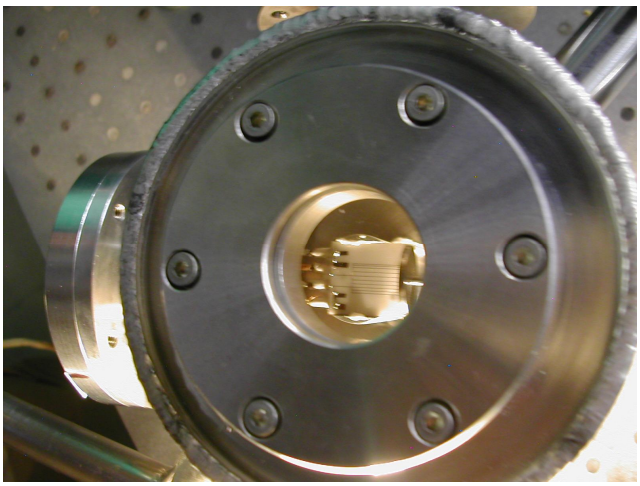

Fig. 4.5. Strip-type electrode placed inside the vacuum chamber.

Figure 4.6 shows optical images of the electric field distribution for the strip-type electrode when all strips are connected to the same potential and when one strip grounded while the remaining strips are held at a fixed potential. Figure 4.7 depicts optical images of an electric field distribution for the same electrode at different voltage values with one strip grounded. The polarization of both laser beams and the polarization of the observed radiation with respect to the electric field direction for the experiment with the strip-type electrode was the same as in the experiment with sealed glass cell with transparent electrodes [dis2] (experimental geometry *zyx*, see chapter 2.3.2) Thus, the magnitude of the signals for the *zyx* geometry obtained with transparent electrodes Fig. 2.6(a) and with the strip-type electrode

(see Figs. 4.6 - 4.7) could be compared at different electric field values. A decrease in LIF intensity of about 12 % at 2000 V/cm for the transparent electrode gives good agreement with the observations for the strip-type electrode. This allows one to apply the theoretical model of the LIF intensity dependence on the external electric field developed in [dis2, dis4] to transform optical signals into images of electric field distributions.

The present work was done in the framework of the NATO Science for Peace Project (No. SfP978029) "***Fast Optical Non-Contact Electric Field Mapping for Semiconductor Technologies***". Detailed information about this project is given in a ***Final Report***.

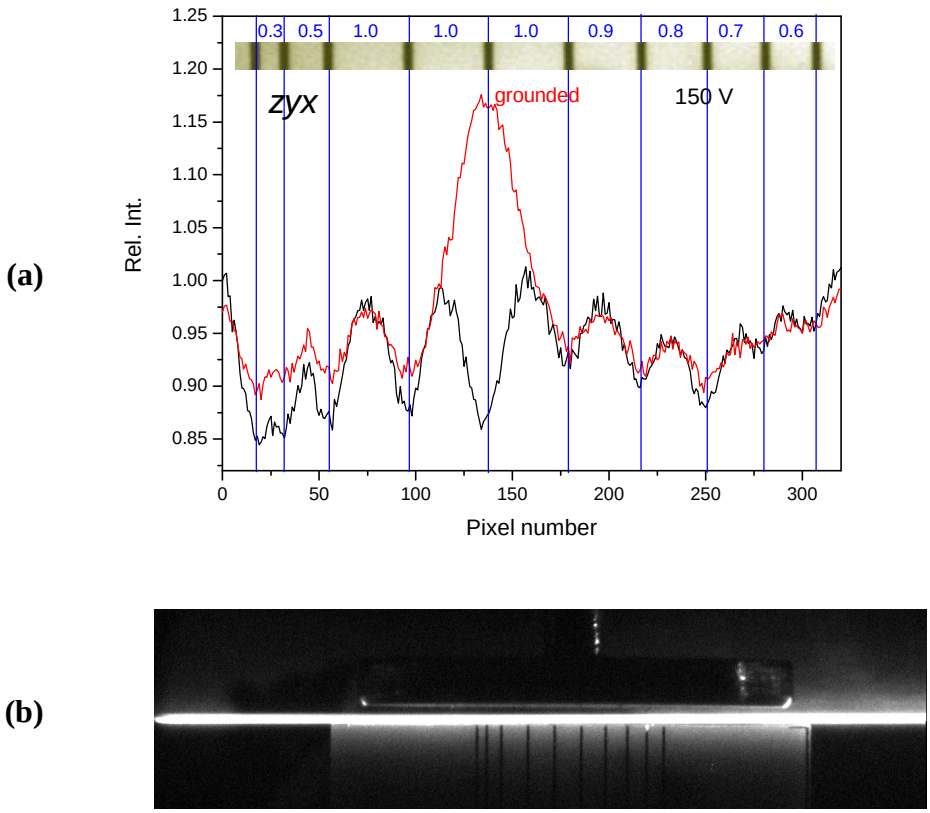

Fig. 4.6. Images of LIF intensities showing electric field distributions. (a) Digitised line averaged profiles of CCD images: black line –150V applied to each strip electrode; red line – same configuration with one of the central electrodes grounded. In the upper part of (a) the strip topology with spacing between strips (in mm) is shown. The blue vertical lines show the consistency between strip and dip position; (b) CCD image of the geometry of the laser beam between the grounded electrode and co-planar strip electrodes.

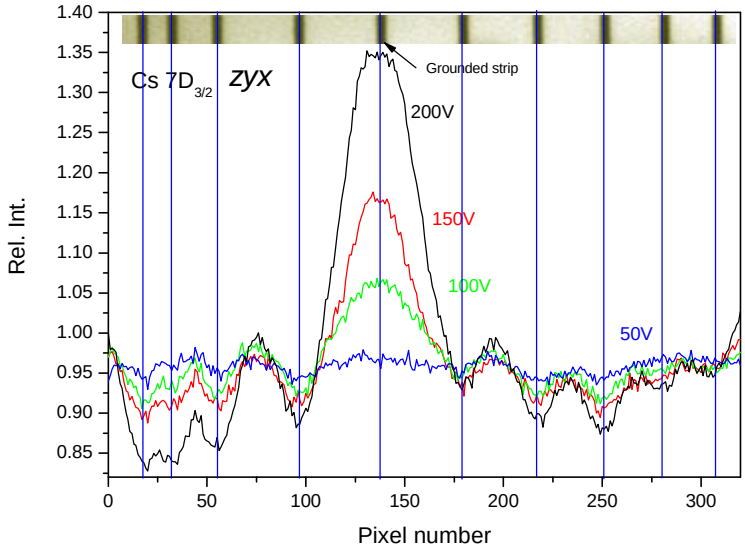

Fig. 4.7. Digitised line average profiles of CCD images of LIF intensities showing how the electric field distribution between the electrodes depends on the applied voltage.

4.3 Conclusions

- The possibility of using Cs vapour as a tracer gas to optically image an external electric field distribution has been demonstrated.
- Optical images of electric field distributions for two different electrode configurations have been obtained, with a spatial resolution on the order of 0.3 mm.
- The sensitivity of the external electric field of the present method mainly depends on which *n*D state of the Cs atom is used for electric field mapping. For $n = 7$ it is hundreds of V/cm and for $n = 9$ and 10, tens of V/cm.

5. NaRb molecules diode laser spectroscopy of the A^1S^+ - b^3P complex

5.1 Background

The spin–orbit (SO) interaction between the first excited singlet state and the second triplet state of alkali dimers has been known for almost a century as a textbook example of perturbation of the rovibronic structure [65]. Since then many spectroscopic studies of the $A^1\Sigma^+ - b^3\Pi$ complex have appeared for homonuclear diatomic molecules Li_2 [66–69], Na_2 [70-75], K_2 [76-79] and Rb_2 [80]. Detailed experimental studies on the $A^1\Sigma^+$ and $b^3\Pi$ states of mixed alkali dimers (see Fig. 5.1 for NaRb) have been performed on NaK by Ross and co-workers [81–83] and on NaRb by the Riga group and co-workers [84].

The SO interaction in the excited states of the NaRb dimmer, which converges to the Rb 5^2P atom, is so strong that the states $A^1\Sigma^+$ and $b^3\Pi$ can be considered, from the point of wiev of energy, as fully mixed even near equilibrium distances. This leads to non-regular energy spacing of the rovibrational levels, when the singlet–triplet perturbation overwhelms the first vibrational differences as well as the rotational and centrifugal distortion.

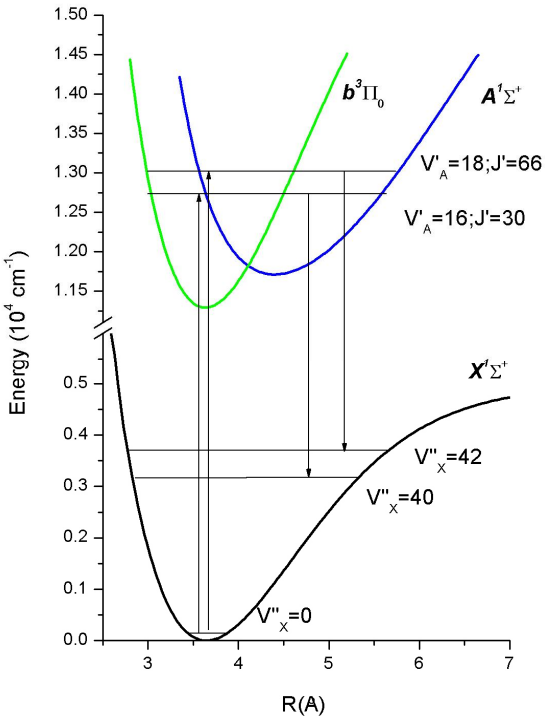

Fig. 5.1. Potential energy curves for the ground state $X\ ^1\Sigma^+$ and the $A\ ^1\Sigma^+ - b^3\Pi$ complex of NaRb.

The inverted channel-coupling approach (ICCA) has been successfully applied in [84] to perform a deperturbation analysis of the $A\ ^1\Sigma^+ - b^3\Pi$ complex of the NaRb molecule. This

approach incorporates the following data: (i) accurate sub-Doppler wave numbers, (ii) LIF intensity measurements (iii) *ab initio* fine structure calculations. The ICCA method, however, becomes feasible only if accurate *ab initio* calculations of the respective spin–orbit coupling electronic matrix elements are available over a wide range of the internuclear distances. It is, therefore, of particular importance to select these molecular properties that are the least sensitive to state mixing, and thus allow the adiabatic approximation to be explored.

The relative intensity distribution $I(v'')$ in the laser induced fluorescence (LIF) spectra is a well-known tool for studying both bound and unbound low-lying excited states of diatomic molecules. Full LIF progressions belonging to a non-diagonal electronic system are useful for establishing the vibrational numbering v' of the excited state by the reflection method [85] since the number of observed maxima in the LIF intensity distribution has to be equal to $v' + 1$ because of the oscillation theorem [86]. Moreover, it was recently proven [87] that the relative intensity distribution $I(v'')$ in long LIF series of a strongly non-diagonal bound–bound system is a powerful tool for restoring the potential energy curve (PEC) of the upper electronic state. This method is very useful when there is a lack of experimental energy data for this state, while an accurate PEC for the lower state and the corresponding transition dipole moment are available.

The main goal of the [dis1] was to measure the LIF intensity distribution from the strongly coupled singlet–triplet NaRb *A*–*b* complex to the ground state by applying diode laser excitation and to demonstrate the applicability of this intensity distribution for direct restoration of the adiabatic PEC of the singlet $A^1\Sigma^+$ state.

5.2 NaRb $A^1\Sigma^+$ - $b^3\Pi$ complex: LIF intensity distribution as a deperturbation tool [dis1]

5.2.1 Experimental setup

NaRb molecules were formed from a 1:4 mixture (by weight) of ^{23}Na and natural Rb (containing 72% of ^{85}Rb and 28% of ^{87}Rb isotopes) metals in an alkali-resistant glass cell. The cell was carefully degassed at a temperature of about 680K and sealed off after filling with metals by distillation. The working temperature was fixed at about 580 K.

The $A^1\Sigma^+ - b^3\Pi \leftarrow X\ ^1\Sigma^+$ transitions to the selected upper state rovibronic levels were induced by a current/temperature stabilized single mode 50 mW diode laser (Hitachi-HL7851C laser diode). Optical feedback from a diffraction grating was used to provide a narrow-band tunable laser output within a spectral range between ca. 780 nm and 790 nm.

The LIF was observed perpendicular to the laser beam and dispersed by a monochromator MDR-3 (600 mm^{-1} diffraction grating blazed for the IR spectral region) in the near-infrared 790-1200 nm spectral range and detected by a FEU-83 photomultiplier tube (PMT) operated in a lock-in regime. During the experiment the PMT was cooled down to -50 °C by the liquid nitrogen vapour flow. The spectral sensitivity of the detection system was calibrated by a standard tungsten band-lamp with known spectral irradiance at definite temperature. The spectral calibration was made by Ne discharge lines which ensured ca. 0.05 nm spectral accuracy that appeared to be satisfactory for unambiguous ground state v''_X, J'' numbering based on the ground state molecular constants from [88].

5.2.2 Results

An example of experimental LIF spectra is given in Fig. 5.2. The continuous background present in the LIF spectra in the $\lambda > 900$nm region is due to rather high alkali vapour pressure and is most probably connected with Rb_2 bands, while the behavior near 800nm is influenced by strong Rb atom resonance transitions. The excited state term values ($T_{v'_A = 16,\ J' = 30}$ = 12802 cm^{-1} and $T_{v'_A = 18,\ J' = 66}$ = 13084 cm^{-1} of $^{23}Na^{85}Rb$ molecule were evaluated by adding the exciting diode-laser wave numbers to the corresponding ground state term values calculated with the refined molecular constants from Ref. [89].

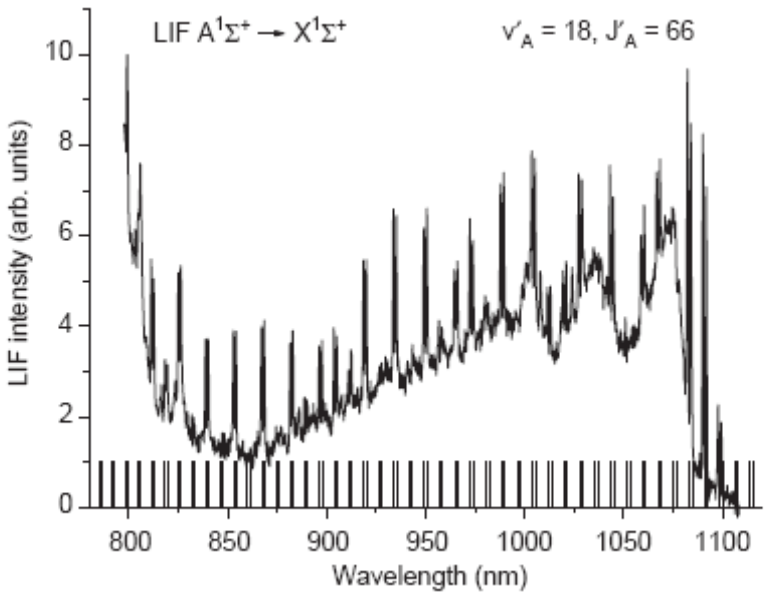

Fig. 5.2. Example of NaRb LIF spectrum obtained by excitation $A\ ^1\Sigma^+(v'_A, J') \leftarrow X\ ^1\Sigma^+(v''_X = 0, J'')$ transitions. v'_A = 18, J' = 66 (P-transition, λ_{exc} = 786,3 nm). The grid represents the positions of the calculated doublets of vibrational progression numbered by v''_X according to Ref. [89].

The experimentally obtained relative intensity distributions of two measured LIF progressions are given in Fig. 5.3. The background and spectral sensitivity of the registration system have been taken into account.

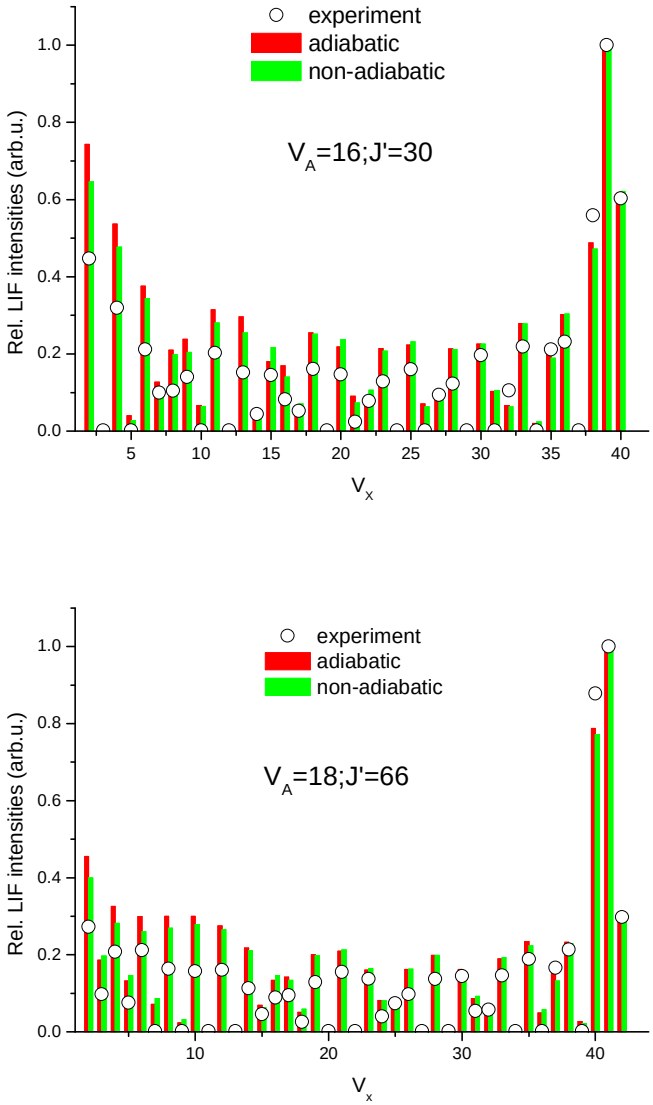

Fig. 5.3. Comparison of experimental LIF intensity distributions with their adiabatic and non-adiabatic counterparts.

The parameters of the adiabatic PEC of the $A^1\Sigma^+$ state restored from the experimentally measured LIF intensity distributions originating from the v'_A = 16 and 18 vibrational levels of the *A*-state are given in Table 5.1. As follows from the table, the present *A*-state molecular constants are in reasonable agreement with the ones obtained in Ref. [84] by involving about 200 *A*-state experimental rovibronic term values (obtained by involving transition frequencies measured with 0.003cm^{-1} accuracy) and exploring much more complicated non-adiabatic ICCA procedure. The sum of the derived Hulburt–Hirschfelder (HH)

electronic and dissociation energy $T_{e_A}^{HH} + D_{e_A}^{HH} = 17535 cm^{-1}$ is consistent with the experimental estimate $D_{e_X}^{exp} + \Delta E^{exp}[Rb(5p^2P_{1/2}) - Rb(5s^2S_{1/2}) = 17609.8 cm^{-1}$ according to $D_{e_X}^{exp}$ from [89] and E[Rb($5^2P_{1/2}$)] from [91].

To confirm the validity of the adiabatic approximation for the LIF intensities, the relevant nonadiabatic Iv_A,v_X values were estimated by using data from [84]. As expected, the non-adiabatic intensities are very close to their adiabatic counterparts for all transitions (see Fig. 5.3). The calculated and measured intensities are in reasonable agreement, their discrepancy are most likely connected with the inaccuracy of the calibration of the spectral sensitivity of the registration system.

Table 5.1. Deperturbed molecular constants for the $A^1\Sigma^+$ state of $^{23}Na^{85}Rb$ (T_e, w_e and D_e in cm^{-1}, a, b are dimensionless, R_e is in A).

T_e	R_e	w_e
Ab initio potentials [90, 84]		
11396	4.47	66.4 [90]
12109	4.24	77.1 [84]
Present "difference based" potentials		
11630	4.38	64.8 [90]
11768	4.45	65.7 [84]
Present adiabatic Hulburt–Hirschfelder model		
11709	4.423	63.51
D_e	5826	
a	5.2735	
b	0.1465	
Non-adiabatic ICCA model [84]		
11702.2	4.406	66.01

5.2.3 Conclusions

- Diode laser radiation has been applied to excite selected rovibronic levels of the strongly coupled singlet-triplet complex $A^1\Sigma^+ - b^3\Pi$ of the NaRb molecule.
- Two almost complete LIF progressions originated from the $A^1\Sigma^+ - b^3\Pi$ complex ($v' = 16$, $J' = 30$ and $v' = 18$, $J' = 66$) to the $X^1\Sigma^+$ ground state ($v'' = 2…42$) and were observed in the near-infrared spectral range from 790 to 1200 nm. Their relative intensity distributions have been obtained.
- The relative intensity distribution in the LIF progressions that originate from the $A^1\Sigma^+ - b^3\Pi$ complex of states completely mixed by the spin-orbit interaction is much less subject to perturbations than the term values. Thus, this distribution may supply a unique clue for performing a partial deperturbation analysis of the strongly mixed states by providing the unambiguous vibrational numbering as well as the adiabatic PEC that can be used as the first approximation for further non-adiabatic treatment.

6. Conclusions

Consistant with the goals of the present work, the following main results have been obtained:

- Electric field induced level-crossing signals of m_F magnetic sublevels of the hyperfine F levels have been observed for the first time when applying two-step laser excitation. Experimentally obtained level-crossing signals for the Cs nD$_{3/2}$ and nD$_{5/2}$ states, with n = 7, 9, and 10 are described theoretically using a correlation analysis of the optical Bloch equations in the case when an atom simultaneously interacts with two laser fields in the presence of an external electric field. New values of the tensor polarizabilities α_2 for the 7 and 9 D$_{3/2}$ states of Cs and the hyperfine structure constants A for the 7, 9 and 10D$_{5/2}$ states of Cs have been determined by means of measured level-crossing signals and detailed theoretical description of these signals.

- Alignment to orientation conversion signals induced by an external electric field have been observed for the first time in atoms, in the 7D$_{3/2}$ and 9D$_{3/2}$ states of Cs. The experimentally obtained signals are described accurately by a detailed theoretical model based on correlation analysis of optical Bloch equations. The phenomenon of AOC deforms distributions of atomic angular momentum in a way that could mimic the signature of an electron electric dipole moment (EDM), and therefore contitutes a potential background for EDM searches in atomic or molecular systems. The present investigation shows that AOC can be understood very well and corrections could be made if necessary.

- The possibility of using Cs vapour as a tracer gas to optically image an external electric field distribution has been demonstrated. Optical images of electric field distributions for two different electrode configurations have been obtained with a spatial resolution of order 0.3 mm. The sensitivity of the external electric field of the method mainly depends on which nD state of the Cs atom is used for electric field mapping. For n = 7 it was hundreds of V/cm, and for n = 9 and 10 it was tens of V/cm.

- Diode laser radiation has been applied to excite selected rovibronic levels of the strongly coupled singlet-triplet complex $A^1\Sigma^+ - b^3\Pi$ of the NaRb molecule. Two nearly complete LIF progressions that originated from the $A^1\Sigma^+ - b^3\Pi$ complex to the $X^1\Sigma^+$ ground state were observed in the near-infrared spectral range and their relative intensity distributions

were obtained. The moderately accurate Hulburt-Hirschfelder potential has been constructed for the $A^1\Sigma^+$ state by means of a direct potential fit analysis of the experimental intensity distributions.

Concluding remarks

The present work has demonstrated that:

- level-crossing spectroscopy within the hyperfine manifold in an external dc electric field can be used as an experimental means to determine atomic properties such as the tensor polarizability α_2 or the hyperfine structure constants A. In particular, highly excited states can be studied when two-step laser excitation is applied.

- electric field induced alignment to orientation conversion can represent a potential background for electron electric dipole moment searches in atomic or molecular systems. Our investigation shows that this phenomenon can be understood very well and corrections could be made, if necessary.

- atomic cesium vapour is a suitable tracer gas for optical imaging of an electric field distribution, which offers the following advantages: low working temperatures, the possibility to implement the method using only diode lasers, and the ease of separating atomic fluorescence from scattered light using simple optical filters.

- The relative intensity distribution from selectively excited rovibronic levels of a mixed singlet-triplet complex of alkali diatomic molecules is a powerful tool for studying fully-mixed states. By means of a temperature and current stabilized diode laser to excite the complex and a low resolution monochromator to observe the fluorescence it is possible to obtain a reliable result.

Appendix A: Experimental and theoretical values of the scalar and tensor polarizabilities of Cs.

State	α_0 exp		α_0 theor		α_2 exp		α_2 theor	
	MHz/(kV/cm)^2	a_0^3	MHz/(kV/cm)^2	a_0^3	MHz/(kV/cm)^2	a_0^3	MHz/(kV/cm)^2	a_0^3
$6^2S_{1/2}$	0.1063(77) [g] 0.1000(20) [h] **0.09978(15) [i]**	427(31)* [g] 402(8)* [h] **401.0(0.6)* [i]**	0.098 [l]	394 * [l]				
$7^2S_{1/2}$			1.528 [l]	6.14×10^3 * [l]				
$8^2S_{1/2}$			9.431 [l]	3.79×10^4 * [l]				
$9^2S_{1/2}$			38.07 [l]	1.53×10^5 * [l]				
$10^2S_{1/2}$	123(6)* [a] 119.06(28)* [f]	$4.94(24)\times10^5$ [a] $4.7848(113)\times10^5$ [f]	118.2 [l]	4.75×10^5 * [l]				
$11^2S_{1/2}$	322(16)* [a] 309.70(26)* [f]	$1.294(64)\times10^6$ [a] $1.2446(11)\times10^6$ [f]	308.6 [l]	1.24×10^6 * [l]				
$12^2S_{1/2}$	720(45)* [a] 713.48(58)* [f]	$2.894(181)\times10^6$ [a] $2.8674(23)\times10^6$ [f]	706.7 [l]	2.84×10^6 * [l]				
$13^2S_{1/2}$	1650(170)* [a] 1491.20(122)* [f]	$6.631(680)\times10^6$ [a] $5.9929(49)\times10^6$ [f]	1468 [l]	5.90×10^6 * [l]				
$6^2P_{1/2}$	$\alpha_0(6^2P_{1/2})$- $\alpha_0(6^2S_{1/2})$ 0,230438 (30)* [e] $\alpha_0(6^2P_{1/2})$- $\alpha_0(6^2S_{1/2})$ 0.2415(24) [d]	$\alpha_0(6^2P_{1/2})$- $\alpha_0(6^2S_{1/2})$ 926,094 (121) [e] $\alpha_0(6^2P_{1/2})$- $\alpha_0(6^2S_{1/2})$ 970.4(9.5)* [d]	0.321 [l]	1.29×10^3 * [l]				
$6^2P_{3/2}$	0.398(60)* [a] $\alpha_0(6^2P_{3/2})$- $\alpha_0(6^2S_{1/2})$ 0.3086(60) [c] $\alpha_0(6^2P_{3/2})$- $\alpha_0(6^2S_{1/2})$ 0.3145(32) [d]	$1.600(241)\times10^3$ [a] $\alpha_0(6^2P_{3/2})$- $\alpha_0(6^2S_{1/2})$ 1240.2(24)* [c] $\alpha_0(6^2P_{3/2})$- $\alpha_0(6^2S_{1/2})$ 1263.9(12.8)* [d]	0.398 [l]	1.60×10^3 * [l]	- 0.065(10)* [a] - 0.0653(4) [c] - 0.0648(20) [d]	- 261.2(40.2) [a] - 262.4(15)* [c] - 260.5(8.1)* [d]	- 0.056 [l]	-2.23×10^2 * [l]
$7^2P_{1/2}$			7.316 [l]	2.94×10^4 * [l]				
$7^2P_{3/2}$			9.182 [l]	3.69×10^4 * [l]	- 1,077(43)* [k]		- 1.065 [l]	-4.28×10^3 * [l]
$8^2P_{1/2}$			54.99 [l]	2.21×10^5 * [l]				
$8^2P_{3/2}$			70.17 [l]	2.82×10^5 * [l]	- 7.6(3)* [a]		- 7.52 [l]	-3.02×10^4 * [l]
$7^2D_{3/2}$	- 14.9(20) [j]	$-6,0(8)\times10^4$* [j]	- 16.22 [l] **- 16.62(40) [dis4]**	-6.52×10^4 * [l] **$-6.68(16)\times10^4$ * [dis4]**	16.42(75) [j] **18.54(50) [dis2]**	$6.6(3)\times10^4$* [j] **$7.45(20)\times10^4$ *[dis2]**	17.52 [l] **17.72(30) [dis4]**	7.04×10^4 * [l] **$7.12(12)\times10^4$ * [dis4]**
$7^2D_{5/2}$	- 18.9(20) [j]	$-7.6(8)\times10^4$* [j]	- 21.67 [l] **- 22.15(47) [dis4]**	-8.71×10^4 * [l] **$-8.90(19)\times10^4$ * [dis4]**	32.1(10) [j]	$1.29(4)\times10^5$* [j]	34.84 [l] **35.28(42) [dis4]**	1.40×10^5 * [l] **$1.418(17)\times10^5$ * [dis4]**

$8^2D_{3/2}$			- 91.1 [l]	- 3.66×10^5 * [l]	82.5(4.0)* [a]	$3.32(16)\times10^5$ [a]	83.6 [l]	3.36×10^5 * [l]
$8^2D_{5/2}$			- 117.5 [l]	- 4.72×10^5 * [l]	182(10)* [a]	$7.31(40)\times10^5$ [a]	168.0 [l]	6.75×10^5 * [l]
$9^2D_{3/2}$	- 360(30)* [a]	- $1.45(12)\times10^6$ [a]	- 348.4 [l] **- 349.1(3.0) [dis4]**	- 1.40×10^6 * [l] **- $1.403(12)\times10^6$ * [dis4]**	313(15)* [a] **294(9)´10^6[dis2]**	$1.258(60)\times10^6$ [a] **$1.183(35)\times10^6$*[dis2]**	296.1 [l] **296.1(2.5) [dis4]**	1.19×10^6 * [l] **$1.190(10)\times10^6$ * [dis4]**
$9^2D_{5/2}$	- 509(25)* [a]	- $2.05(10)\times10^6$ [a]	- 440 [l] **- 442.2(3.5) [dis4]**	- 1.77×10^6 * [l] **- $1.777(14)\times10^6$ * [dis4]**	660(35)* [a]	$2.65(14)\times10^6$ [a]	592.2 [l] **593.7(3.2) [dis4]**	2.38×10^6 * [l] **$2.386(13)\times10^6$ * [dis4]**
$10^2D_{3/2}$	- 1150(170)* [a] - 1041.3(0.9)* [b]	- $4.622(683)\times10^6$ [a] - $4.185(4)\times10^6$ [b]	- 1050 [l] **- 1054.0(7.2) [dis4]**	- 4.22×10^6 * [l] **- $4.236(29)\times10^6$ * [dis4]**	840(40)* [a] 846.3(0.9)* [b]	$3.376(160)\times10^6$ [a] $3.4012(36)\times10^6$ [b]	848 [l] **850.0(6.0) [dis4]**	3.41×10^6 * [l] **$3.416(24)\times10^6$ * [dis4]**
$10^2D_{5/2}$	- 1340(130)* [a] - 1319.5(2.1)* [b]	- $5.385(522)\times10^6$ [a] - $5.303(8)\times10^6$ [b]	- 1319 [l] **- 1322.8(9.0) [dis4]**	- 5.30×10^6 * [l] **- $5.316(36)\times10^6$ * [dis4]**	1770(90)* [a] 1695.7(4.9)* [b]	$7.113(360)\times10^6$ [a] $6.8148(197)\times10^6$ [b]	1704 [l] **1708.7(8.0) [dis4]**	6.85×10^6 * [l] **$6.867(32)\times10^6$ * [dis4]**
$11^2D_{3/2}$	- 2694.6(2.7)* [b]	- $1.0829(11)\times10^7$ [b]	- 2712 [l]	- 1.09×10^7 * [l]	2107.5(2.7)* [b]	$8.4697(109)\times10^6$ [b]	2120 [l]	8.52×10^6 * [l]
$11^2D_{5/2}$	- 3790(350)* [a] - 3379.5(5.4)* [b]	- $1.523(141)\times10^7$ [a] - $1.3582(22)\times10^7$ [b]	- 3384 [l]	- 1.36×10^7 * [l]	4010(400)* [a] 4242.1(11.4)*[b]	$1.612(161)\times10^7$ [a] $1.7048(46)\times10^7$ [b]	4255 [l]	1.71×10^7 * [l]
$12^2D_{3/2}$	- 6180(4.9)* [b]	- $2.484(2)\times10^7$ [b]	- 6245 [l]	- 2.51×10^7 * [l]	4691.4(4.9)* [b]	$1.8854(197)\times10^7$ [b]	4753 [l]	1.91×10^7 * [l]
$12^2D_{5/2}$	- 7660(15)* [b]	- $3.078(6)\times10^7$ [b]	- 7738 [l]	- 3.11×10^7 * [l]	9501(39)* [b]	$3.8183(157)\times10^7$ [b]	9530 [l]	3.83×10^7 * [l]
$13^2D_{3/2}$	- 12935(18)* [b]	- $5.1984(72)\times10^7$ [b]	- 12989 [l]	- 5.22×10^7 * [l]	9620(18)* [b]	$3.8661(72)\times10^7$ [b]	9679 [l]	3.89×10^7 * [l]
$13^2D_{5/2}$	- 16001(25)* [b]	- $6.431(10)\times10^7$ [b]	- 16099 [l]	- 6.47×10^{47} * [l]	$19(1)\times10^3$* [a] 19406(49)* [b]	$7.64(40)\times10^7$ [a] $7.7990(197)\times10^7$ [b]	19533 [l]	7.85×10^7 * [l]
$14^2D_{5/2}$					$37(2)\times10^3$* [a]	$1.49(8)\times10^8$ [a]		
$15^2D_{5/2}$					$70(4)\times10^3$* [a]	$2.81(16)\times10^8$ [a]		
$16^2D_{5/2}$					$120(6)\times10^3$* [a]	$4.82(24)\times10^8$ [a]		
$17^2D_{5/2}$					$199(10)\times10^3$* [a]	$8.00(40)\times10^8$ [a]		
$18^2D_{5/2}$					$323(16)\times10^3$* [a]	$1.298(64)\times10^9$ [a]		

* Shows in which units the polarizability values were given in the paper.
The atomic units $\mathbf{a_0^3}$ can be converted to the SI units **MHz/(kV/cm)^2** via $\alpha[\text{MHz/(kV/cm)}^2] = 2.48828\times10^{-4}\ \alpha[a_0^3]$
Correspondingly, the SI units can be converted to the atomic units via $\alpha[a_0^3] = 4.01884\times10^3\ \alpha[\text{MHz/(kV/cm)}^2]$

[a] K. Fredriksson and S. Svanberg, Z. Phys. A 281, 189 (1977).
The scalar polarizability constant a_0 for excited S and D states in cesium was measured utilizing a two-step excitation scheme. An rf lamp and a single-mode dye laser were used to excite the atoms in a collimated atomic beam. Tensor polarizabilities of all D-states have been measured by level-crossing spectroscopy except for $11^2D_{5/2}$.

[b] J. Xia, J. Clarke, J. Li, and W. A. van Wijngaarden, Phys. Rev. A **56**, 5176-5178 (1997)
The scalar and tensor polarizabilities of the cesium (10–13)$D_{3/2,5/2}$ states were found with uncertainties of less than 0.3%. Stark shifts were determined using an electro-optically modulated laser beam. This experiment measured the voltage required for atoms excited by a laser beam in an electric field to be simultaneously in resonance as atoms excited by a frequency sideband of the laser in a field-free region.

[c] C. E. Tanner and C. Wieman, Phys. Rev. A **38**, 162 (1988).
The Stark shift of the $6P_{3/2}$ state relative to the ground state of atomic cesium was measured by means of crossed-beam laser spectroscopy with a frequency-stabilized laser diode. The scalar and tensor polarizabilities were determined from the Stark shifts measured in the transitions $6S_{1/2}$ F = 4 → $6P_{3/2}$ F' = 5, m_F = 5 and 4.

[d] L. R. Hunter, D. Krause Jr., S. Murthy, and T. W. Sung, Phys. Rev. A **37**, 3283 (1988).
The dc Stark shift of the cesium D lines was observed in the low-field limit where the induced shift is small compared to the various hyperfine splittings. On the D2 line, the modification by the electric field of the dipole transition rates to the various excited-state hyperfine levels must be taken into account in order to interpret results.

[e] L. R. Hunter, D. Krause, Jr. and K. E. MillerD. J. Berkeland and M. G. Boshier, Opt. Commun. 94, 210 (1992).
The dc Stark shift of the cesium D1 line was observed using two 894 nm cavity-stabilized diode lasers locked to resonance signals from an atomic beam and a saturated absorption cell. The heterodyne signal obtained from the two lasers and optical measurement of the electrode spacing allowed well calibrated high precision measurements to be made. The observed scalar shift was found to be 115.219 (15) kHz $(kV/cm)^{-2}$. We believe this result to be the most precise Stark shift measurement ever reported.

[f] W. A. van Wijngaarden *E.* A. Hessels, J. Li, and N. E. Rothery, Phys. Rev. A **49**, R2220 (1994).
The scalar polarizabilities of the cesium (10–13)$S_{1/2}$ states were measured with accuracies of better than 0.1%. The Stark shifts were measured using two atomic beams. One traverses a uniform electric field and the other crosses a field-free region. The atoms were excited using a ring dye laser. Frequency shifted by an acousto-optic modulator the laser beam interacting with the atoms in the electric-field region. The Stark field was determined by measuring the electric field for which the atoms in both beams were simultaneously in resonance.

[g] W. D. Hall and J. C. Zorn, Phys. Rev. A **10**, 1141-1144 (1974)
The electric dipole polarizability of the alkali-metal atoms Na, K, Rb, and Cs were determined by measuring the deflection of a velocity-selected beam by an inhomogeneous electric field.

[h] R. W. Molof, H. L. Schwartz, T. M. Miller, and B. Bederson, Phys. Rev. A **10**, 1131-1140 (1974)
The E-H-gradient balance technique has been used to measure the static electric dipole polarizabilities of the alkali-metal atoms.

[i] J. M. Amini and H. Gould, Phys. Rev. Lett. **91**, 153001 (2003)
The cesium $6^2S_{1/2}$ scalar dipole polarizability $alpha_0$ was determined from the time-of-flight of laser cesium atoms that were laser cooled and launched through an electric field. They found $a_0 = 6.611 \pm 0.009 \times 10^{-39}\ C\ m^2/V = 59.42 \pm 0.08 \times 10^{-24}\ cm^3 = 401.0 \pm 0.6\ a^3_0$. The 0.14% uncertainty is a factor of 14 improvement over the previous measurement.

[j] J. E. Wessel and D. E. CooperPhys. Rev. A **35**, 1621-1627 (1987)
Stark spectroscopy and Autler-Townes interactions in four-level cesium atoms.
Scalar and tensor polarizabilities of cesium 5*f* and 7*d* states were measured by three-color multiphoton excitation techniques.

[k] A. Khadjavi, A. Lurio, and W. Happer, Phys. Rev. 167, 128 (1968)
The method of pure electric field level crossing.

[l] W. A. van Wijngaarden and J. Li, J. Quant. Spectrosc. Radiat. Transf. **52**, 555 (1994).
The scalar and tensor polarizabilities of over sixty S, P, D and F states of cesium were evaluated using the Coulomb approximation.

References

[1] M. Stuke (Ed.): 25 Years Dye Laser, Topics Appl. Phys., Vol. 70 (Springer, Berlin, Heidelberg 1992).

[2] W. Hanle, Z. Physik **30**, 93 (1924).

[3] W. Happer, Rev. Mod. Phys. **44**, 168 (1972).

[4] G. Belin, L. Holmgren, I. Lindgren, S. Svanberg, Phys. Scr. **12,** 287 (1975).

[5] G. Belin, L. Holmgren, S. Svanberg, Phys. Scr. **13,** 351 (1976).

[6] G. Belin, L. Holmgren, S. Svanberg, Phys. Scr. **14**, 39 (1976).

[7] A. Khadjavi, W. Happer Jr., A. Lurio, Phys. Rev. Lett. **17**, 463 (1966).

[8] A. Khadjavi, A. Lurio, W. Happer, Phys. Rev. **167**, 128 (1968).

[9] Robert W. Schmieder, Allen Lurio, W. Happer, Phys. Rev. A **3**, 1209 (1971).

[10] I. B. Khriplovich and S. K. Lamoreaux, *CP Violation Without Strangeness* (Springer-Verlag, Berlin, 1997).

[11] P. G. H. Sandars, Contemp. Phys. **42**, 97 (2001).

[12] B. C. Regan, E. D. Commins, C. J. Schmidt, and D. DeMille, Phys. Rev. Lett. **88**, 071805 (2002).

[13] M. Auzinsh, R. Ferber, Optical Polarization of Molecules, Cambridge University Press, Cambridge, 2005.

[14] U. Fano, Phys. Rev. **133**, B828 (1964).

[15] V. N. Rebane, Opt. Spectrosc. (USSR) **24**, 163 (1968).

[16] M. Lombardi, C.R. Seances Acad. Sci., Ser. B **265**, 191 (1967).

[17] M. Lombardi, J. Phys. (Paris) **30**, 631 (1969).

[18] M. Lombardi, in *Beam Foil Spectroscopy, Collisional and Radiative Processes,* edited by I. Sellin and D. Pegg (Plenum Press, New York, 1996), Vol. 2, pp. 731–747.

[19] M. Auzinsh and R. Ferber, Phys.Rev. Lett. **69**, 3463 (1992).

[20] M. Auzinsh, R. Ferber, and A.V. Stolyarov, J. Chem. Phys. **101**, 5559 (1994).

[21] M. Auzinsh, Can. J. Phys. **75**, 853 (1997).

[22] T. Nakajima , N. Uchitomi, Y. Adachi, S. Maeda and C. Hirose, 1983 *J. Phys. Colloq.* C **7** 497

[23] D. Yang, D. Lieberman and P. van der Straten, T. Bergeman, and H. Metcalf, *Phys. Rev.* A **40**, 5026 (1989).

[24] Marcis Auzinsh, Ruvin Ferber, Olga Nikolayeva, Neil Shafer-Ray and Maris Tamanis, J. Phys. D: Appl. Phys. **34**, 624–630 (2001).

[25] M. G. Kozlov and D. DeMille, Phys. Rev. Lett. 89, 133001 (2002).

[26] J. J. Hundson, B. E. Sauer, M. R. Tarbutt, and E. A. Hinds, Phys. Rev. Lett. 89, 023003 (2002).

[27] D. DeMille, Phys. Rev. Lett. 88, 067901 (2002).

[28] C. A. Stan, M. W. Zwierlein, C. H. Schunck, S. M. F. Raupach, and W. Ketterle, Phys. Rev. Lett. **93**, 143001 (2004).

[29] S. Inouye, J. Goldwin, M. L. Olsen, C. Ticknor, J. L. Bohn, and D. S. Jin, Phys. Rev. Lett. **93**, 183201 (2004).

[30] D. Wang, J. Qi, M. F. Stone, O. Nikolayeva, H. Wang, B. Hattaway, S. D. Gensemer, P. L. Gould, E. E. Eyler, and W. C. Stwalley, Phys. Rev. Lett. **93**, 243005 (2004).

[31] M. W. Mancini, G. D. Telles, A. R. L. Caires, V. S. Bagnato, and L. G. Marcassa, Phys. Rev. Lett. **92**, 133203 (2004).

[32] C. Haimberger, J. Kleinert, M. Bhattacharya, and N. P. Bigelow, Phys. Rev. A **70**, 021402(R) (2004).

[33] G. D. Telles, L. G. Marcassa, S. R. Muniz, S. G. Miranda, A. Antunes, C. Westbrook, and V. S. Bagnato, Phys. Rev. A **59**, R23 (1999).

[34] Y. E. Young, R. Ejnisman, J. P. Shaffer, and N. P. Bigelow, Phys. Rev. A **62**, 055403 (2000).

[35] G. D. Telles, L. S. Aguiar, L. G. Marcassa, and V. S. Bagnato, Phys. Rev. A **66**, 025403 (2002).

[36] J. M. Sage, S. Sainis, T. Bergeman, and D. DeMille, Phys. Rev. Lett. **94**, 203001 (2005).

[37] W. C. Stwalley, Eur. Phys. J. D **31**, 221 (2004).

[38] E.B. Aleksandrov, M.P. Chaika, G.I. Khvostenko, Interference of Atomic States: In Springer Series on Atoms and Plasmas, Springer, Berlin (1993).

[39] W.A. Van Wijngaarden, J. Li, J. Quant. Spect. Radiat. Transf. **52**, 555 (1994).

[40] E. Arimondo, M. Inguscio, P. Violino, Rev. Mod. Phys. **49**, 31 (1977).

[41] S. Svanberg, P. Tsekeris, Phys. Rev. A **11**, 1125 (1975).

[42] J.S. Deech, R. Luypaert, G.W. Series, J. Phys. B **8**, 1406 (1975).

[43] J. Xia, J. Clarke, J. Li, W.A. Wijngaarden, Phys. Rev. A **56**, 5176 (1997).

[44] J.E. Wessel, D. Cooper, Phys. Rev. A **35**, 1621 (1987).

[45] K. Fredrikson, S. Svanberg, Z. Physik A **281**, 189 (1977).

[46] K. Blum, *Density Matrix Theory and Applications* (Plenum Press, New York, 1996), 2nd ed.

[47] E. Chamoun, M. Lombardi, M. Carre, and M. L. Gaillard, J. Phys. (Paris) **38**, 591 (1977).

[48] T. Manabe, T. Yabuzaki, and T. Ogawa, Phys. Rev. Lett. **46**, 637 (1981).

[49] R. C. Hilborn, L. R. Hunter, K. Johnson, S. K. Peck, A. Spencer, and J. Watson, Phys. Rev. A **50**, 2467 (1994).

[50] M. Krainska-Miszczak, J. Phys. B **12**, 555 (1979).

[51] J. Alnis and M. Auzinsh, Phys. Rev. A **63**, 023407 (2001).

[52] X. L. Han and G.W. Schinn, Phys. Rev. A **43**, 266 (1991).

[53] O. Nikolayeva, M. Auzinsh, M. Tamanis, R. Ferber, J. Mol. Struct. 283, 480-481 (1999).

[54] R. C. Hilborn, Am. J. Phys. **63**, 330 (1995).

[55] S. M. Rochester and D. Budker, Am. J. Phys. **69**, 450 (2001).

[56] I. Langmuir, J. Franklin Inst. **196**, 751 (1923).

[57] E. Weber, *Electromagnetic Theory* (Dover, New York, 1965).

[58] Y. Hamasaki, H Gotoh, M Katoh and S. Takeuchi, Electron-Lett. **16**, 406 (1980).

[59] S. R. M. Robertson and A. J. Rogers, IEEE Proc. J. 132, 195 (1985).

[60] K. Koo and G. Siegel, IEEE J. Quantum Electron QE-18, 670 (1982).

[61] D. Doughty and J. Lawler, Appl. Phys. Lett. **45**, 611 (1984).

[62] B. N. Ganguly and A. Garscadden, Phys. Rev. A **32**, 2544 (1985).

[63] D. K. Doughty, S. Salih, and J. E. Lawler, Phys. Lett. **103A**, 41 (1984).

[64] Marcis Auzinsh, Lalith Jayasinghe, Lance Oelke, Ruvin Ferber and Neil Shafer-Ray, J. Phys. D: Appl. Phys. **34**, 1933–1938 (2001).

[65] R. W. Wood and F. E. Hackett, Astrophys. J. **30**, 339 (1909).

[66] X. Xie and R. W. Field, Chem. Phys. **99**, 337 (1985).

[67] X. Xie and R. W. Field, J. Mol. Spectrosc. **117**, 228 (1986).

[68] C. Linton, F. Martin, I. Russier, A. J. Ross, P. Crozet, S. Churassy, and R. Bacis, J. Mol. Spectrosc. **175**, 340 (1996).

[69] K. Urbanski, S. Antonova, A. M. Lyyra, A. Yiannopoulou, and W. C. Stwalley, J. Chem. Phys. **104**, 2813 (1996).

[70] J. B. Atkinson, J. Becker, and W. Demtröder, Chem. Phys. Lett. **87**, 92 (1982).

[71] C. Effantin, O. Babaky, K. Hussein, J d'Incan, and R. F. Barrow, J. Phys. B **18**, 4077 (1985).

[72] A. M. Lyyra, H. Wang, T.-J. Whang, L. Li, and W. C. Stwalley, Phys. Rev. Lett. **66**, 2724 (1991).

[73] O. C. Mullins, C. R. Makon, and T. F. Gallagher, Chem. Phys. Lett. **126**, 501 (1986).

[74] H. Kato, M. Otani, and M. Baba, J. Chem. Phys. **89**, 653 (1988).

[75] H. G. Krämer, M. Keil, J. Wang, R. A. Bernheim, and W. Demtröder, Chem. Phys. Lett. **272**, 391 (1997).

[76] A. J. Ross, P. Crozet, C. Effantin, J d'Incan, and R. F. Barrow, J. Phys. B **20**, 6225 (1987).

[77] A. M. Lyyra, W. T. Luh, L. Li, H. Wang, and W. C. Stwalley, J. Chem. Phys. **92**, 43 (1990).

[78] G. Jong, L. Li, T. J. Whang, A. M. Lyyra, W. C. Stwalley, M. Li, and J. Coxon, J. Mol. Spectrosc. **155**, 115 (1992).

[79] J. T. Kim, H. Wang, C. C. Tsai, J. T. Bahns, W. C. Stwalley, G. Jong, and A. M. Lyyra, J. Chem. Phys. **102**, 6646 (1995).

[80] C. Amiot, O. Dulieu, and J. Verge`s, Phys. Rev. Lett. **83**, 2316 (1999).

[81] A. J. Ross, C. Effantin, J. d'Incan, and R. F. Barrow, Mol. Phys. **56**, 903 (1985).

[82] A. J. Ross, C. Effantin, J. d'Incan, and R. F. Barrow, J. Phys. B **19**, 1449 (1986).

[83] A. J. Ross, R. M. Clements, and R. F. Barrow, J. Mol. Spectrosc. **127**, 546 (1988).

[84] M. Tamanis, R. Ferber, A. Zaitsevskii, E. A. Pazyuk, A. V. Stolyarov, Hongmin Chen, Jianbing Qi, H. Wang, W. C. Stwalley, J. Chem. Phys. **117**, 7980–8 (2002).

[85] J. Tellinghuisen, The Franck–Condon principle in bound-free transitions, photodissociation and photoionization. New York: Wiley, p. 299–369 (1986).

[86] L. D. Landau, E. M. Lifshitz Quantum mechanics, Non-relativistic theory. New York: Pergamon Press, p. 617 (1965).

[87] A. Zaitsevskii, S. O. Adamson, E. A. Pazyuk, A. V. Stolyarov, O. Nikolayeva, O.Docenko, I. Klincare, M. Auzinsh, M. Tamanis, R. Ferber, R. Cimiraglia, Phys Rev A **63**, 052504 (2001).

[88] O. Docenko, O. Nikolayeva, M. Tamanis, R. Ferber, E. A. Pazyuk, A. V. Stolyarov, Phys. Rev. A **66**, 502508 (2002).

[89] O. Docenko, M. Tamanis, R. Ferber, A. Pashov, H. Knockel, E. Tiemann, Phys. Rev. A **69**, 042503 (2004).

[90] M. Korek, A. R. Allouche, M. Kobeissi, A. Chaalan, M. Dagher, K. Fakherddin, M. Aubert-Frecon, Chem. Phys. **256**, 1 (2000).

[91] Moore CE. Atomic energy levels. NSRDS – NBS 35/VII. US National Bureau of Standards, p. 180. (1971).

Acknowledgments

First of all, I would like to express my gratitude to my scientific supervisor Prof. Ruvin Ferber for his never-ending enthusiasm, which inspired me to start this work and also for helping me to carry it through. I am extremely grateful to Dr. Maris Tamanis and Dr. Florian Gahbauer in cooperation with whom all experiments were done, for a lot of discussion, for useful advice. I am indebted to Prof. Marcis Auzinsh for encouraging me to study coherent effects in atoms and for his efforts to push forward the research in this field at our institute. I also would like to thank Dr. Kaspar Bluss for the calculations with the theoretical model. A special thank to Dr. Janis Alnis, who guided me into the field of diode laser spectroscopy. Thanks to Dr. Robert Kalendarev for producing the glass cells. I am also grateful to all MOLPOL colleagues Dr. Ilze Klincare, Dr Olga Nikolajeva, Dr. Olga Docenko, Jelena Zaharova and Oskars Martinsons for their friendly support.

I acknowledge the support from the University of Latvia and European Social Fund.